SMC-TR-97-09

AEROSPACE REPORT NO.
TR-97(1410)-2

Launch Abort Chemistry Model

8 February 1997

Prepared by

B. B. BRADY, A. MCILROY, and L. R. MARTIN
Mechanics and Materials Technology Center
Technology Operations

Prepared for

SPACE AND MISSILE SYSTEMS CENTER
AIR FORCE MATERIEL COMMAND
2430 E. El Segundo Boulevard
Los Angeles Air Force Base, CA 90245

Space Systems Group

THE AEROSPACE CORPORATION
El Segundo, California

This report was submitted by The Aerospace Corporation, El Segundo, CA 90245-4691, under Contract No. F04701-93-C-0094 with the Space and Missile Systems Center, 2430 E. El Segundo Blvd., Los Angeles Air Force Base, CA 90245. It was reviewed and approved for The Aerospace Corporation by S. Feuerstein Principal Director, Mechanics and Materials Technology Center. Maj. R. Reiners was the project officer for the program.

This report has been reviewed by the Public Affairs Office (PAS) and is releasable to the National Technical Information Service (NTIS). At NTIS, it will be available to the general public, including foreign nationals.

This technical report has been reviewed and is approved for publication. Publication of this report does not constitute Air Force approval of the report's findings or conclusions. It is published only for the exchange and stimulation of ideas.

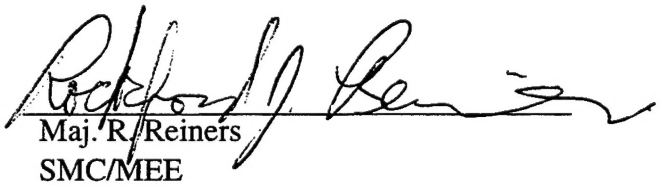

Maj. R. Reiners
SMC/MEE

REPORT DOCUMENTATION PAGE

Form Approved
OMB No. 0704-0188

1. AGENCY USE ONLY (*Leave blank*)	2. REPORT DATE	3. REPORT TYPE AND DATES COVERED
	8 February 1997	

4. TITLE AND SUBTITLE
Launch Abort Chemistry Model

5. FUNDING NUMBERS
F04701-93-C-0094

6. AUTHOR(S)
B. B. Brady, A. McIlroy, and L. R. Martin

7. PERFORMING ORGANIZATION NAME(S) AND ADDRESS(ES)
The Aerospace Corporation
Technology Operations
El Segundo, CA 90245-4691

8. PERFORMING ORGANIZATION REPORT NUMBER
TR-97(1410)-2

9. SPONSORING/MONITORING AGENCY NAME(S) AND ADDRESS(ES)
Space and Missile Systems Center
Air Force Materiel Command
2430 E. El Segundo Boulevard
Los Angeles Air Force Base, CA 90245

10. SPONSORING/MONITORING AGENCY REPORT NUMBER
SMC-TR-97-09

11. SUPPLEMENTARY NOTES

12a. DISTRIBUTION/AVAILABILITY STATEMENT
Approved for public release; distribution unlimited

12b. DISTRIBUTION CODE

13. ABSTRACT (*Maximum 200 words*)

Computer models provide a framework for better understanding of complex phenomena. Events such as launch aborts are rare, and detailed field information about the chemical load they introduce into the atmosphere is rare. A good model will make predictions about the time dependence of the chemical concentra-tions and temperatures in such an event and, therefore, makes it possible to correlate and evaluate incomplete data on chemical observations. A model should make it possible to scale field experiments. For the act-ual event, a good model should predict the statistical likelihood for certain chemical loads to occur, and it should be able to fore-cast the effect of meteorological conditions (e.g., relative humidity, dispersion rate) on the severity of the event.

The launch abort problem is especially difficult because there are separate initial clouds of fuel and oxidizer, with regions of mixing between them. In this report, we deal with this problem with a "multi-bin" approach, which treats the fuel and oxidizer and an interface as separate bins, but keeps the computation tractable. The computer program we use is based on SURFACE CHEMKIN, a standard chemical kinetic subrou-tine package.

The model results show, thus far, that the outcome is highly dependent on initial conditions. However, we feel that a likely scenario for Titan IV will result in 24% of the initial oxidizer remaining, of which at least half is transformed into nitric acid, and 2% of the initial fuel remaining. These source strength numbers are roughly half those given by Lockheed-Martin for hydrazine and oxidizer, and about one-third those presently used for the oxi-dizer in REEDM. If we begin with the assumption presently used in REEDM, i. e., that 70% of the oxidizer remains, then our heterogeneous chemistry model shows that half of that will convert to nitric acid.

14. SUBJECT TERMS	15. NUMBER OF PAGES
Hydrazine, Nitrogen tetroxide, Hypergols, N_2H_4, N_2O_4, UDMH, Aerozine 50, Dispersion, Catastrophic, Environment	55
	16. PRICE CODE

17. SECURITY CLASSIFICATION OF REPORT	18. SECURITY CLASSIFICATION OF THIS PAGE	19. SECURITY CLASSIFICATION OF ABSTRACT	20. LIMITATION OF ABSTRACT
UNCLASSIFIED	UNCLASSIFIED	UNCLASSIFIED	

Contents

Figures

Tables

1. Introduction

A catastrophic launch abort is a complex chemical and physical event, and modeling the source strength for such an event will inevitably be complicated. An abort creates multiple clouds of poorly mixed fuel and oxidizer, and these clouds mix continuously with the surrounding air. This situation may be created by a variety of initial events, and thus many scenarios are possible. One objective of this work is to examine numerous sets of initial conditions with a computer model and to look for patterns of behavior that may permit statistical prediction of the likely source strengths. A good model should make it possible to understand and evaluate information on aborts and should aid in forecasting the environmental impact of such events.

Previous work in this area has been done by S. P. Prince and D. W. Banning of Lockheed Martin.[1] That work was a thermodynamic model of a launch abort. The thermodynamic approach is a necessary first step to understanding the source chemistry, and many important facts and background material are to be found in Reference 1. The limitation of a thermodynamic model, however, is that assumptions must be made about the degree to which chemical reactions go to completion. Because of the rapidly changing concentrations and temperatures in the abort clouds, the progress of many reactions is very difficult to estimate.

A kinetic model can reduce (but not eliminate) the number of assumptions that must be made to predict an outcome. With a full chemical kinetic, adiabatic computer model, the progress of all the chemical reactions in a situation of rapidly diluting and cooling (or burning) can be forecast.

There is a further difficulty, and that is the "multiple cloud," or poorly mixed cloud problem. Most chemical kinetic models deal with a well-mixed initial situation and develop the time dependence of the chemical species in a uniform volume. In order to deal with a poorly mixed situation, we developed the "multi-bin" approach, described in detail below. The idea here is to model separate but gradually mixing clouds of fuel, oxidizer, and air. A fourth "interface" bin is introduced to model the burning region between the fuel and oxidizer clouds. This approach is simple enough to be computationally tractable, but gives essential features of the clouds, such as peak temperatures and the progress of chemical reactions. While more sophisticated CFD-reacting flow models exist, they cannot deal with large sets of chemical reactions as we can. In this regard, we describe this model as having sophisticated chemistry but simplistic mass transport. Further application of this model could involve incorporation of the chemical information into a more elaborate transport model.

2. The Chemical Model—General Considerations

The chemistry in our model involves both atmospheric chemistry and combustion chemistry. The atmospheric chemistry of the hydrazines is based on the smog chamber studies of the early 1980's (Tuazon, et al.[2]). The atmospheric chemistry of nitrogen tetroxide is complicated by heterogeneous reactions that form nitric acid, and we have described this problem in an earlier publication.[3] The NO_2 heterogeneous reaction rates were taken from Park and Lee.[4] Our model results for "cold" nitrogen tetroxide spills indicate that there will be substantial ($\approx$ 90%) conversion of the nitrogen tetroxide to nitric acid by heterogeneous processes. This chemistry is included in the two-bin studies described later. The combustion mechanism for the hydrazines includes gas-phase reactions from the NIST Database[5] and from a standard methane combustion mechanism.[6] Thermodyanmic data are from the JANAF Tables.[7] The complete set of 298 gas-phase reactions and 13 heterogeneous reactions is listed in the Appendix.

The computer model is based on the SURFACE CHEMKIN subroutine package developed by R. J. Kee of Sandia, Livermore.[8,9,10] This package contains subroutines for calculating thermodynamic properties, equilibrium constants, rates, and unit conversions, for parsing character data such as species and element names and reaction mechanisms. The subroutine LSODE (Livermore Solver of Ordinary Differential Equations) is used for solving the set of differential equations. SURFACE CHEMKIN is a set of software tools and a subroutine library designed to help create a program to solve a specific chemical kinetics or thermodynamics problem. The package is designed to help solve a group of differential equations subject to a set of constraints; various properties of the system may be extracted along the way. One needs to write the program that describes the chemical system of interest and calls the appropriate subroutines to do the calculations. Multiple surface and bulk phases can be included. Surface rates are scaled by the ratio of surface area to gas-phase volume. The package is designed to model chemical vapor deposition. We wrote a driver program incorporating some changes in the calculation method, added some new subroutines, and modified some of the original routines. The resulting program is well adapted to atmospheric chemistry. Our alterations are described in more detail below and in the Appendix.

3. The Multi-Bin Approach

Our work began as a representation of a Gaussian plume—the "plume bin"—dispersing in the atmosphere—the "atmosphere bin." This was called a two-bin model. In order to deal with the complex situation of a launch abort, we expanded this to three plume bins: the oxidizer bin, the fuel bin, and the interface bin; and to one atmosphere bin, for a total of four bins. The arrangement of the bins is shown schematically in Figure 1. The atmosphere is much larger than the plume, so the atmospheric composition does not change. The fuel and oxidizer bins mix with the atmosphere and with the interface bin. The interface bin mixes with the fuel and oxidizer bins; it does not mix with the atmosphere except through the fuel and oxidizer bins. The rates of mixing with the atmosphere are assumed to be

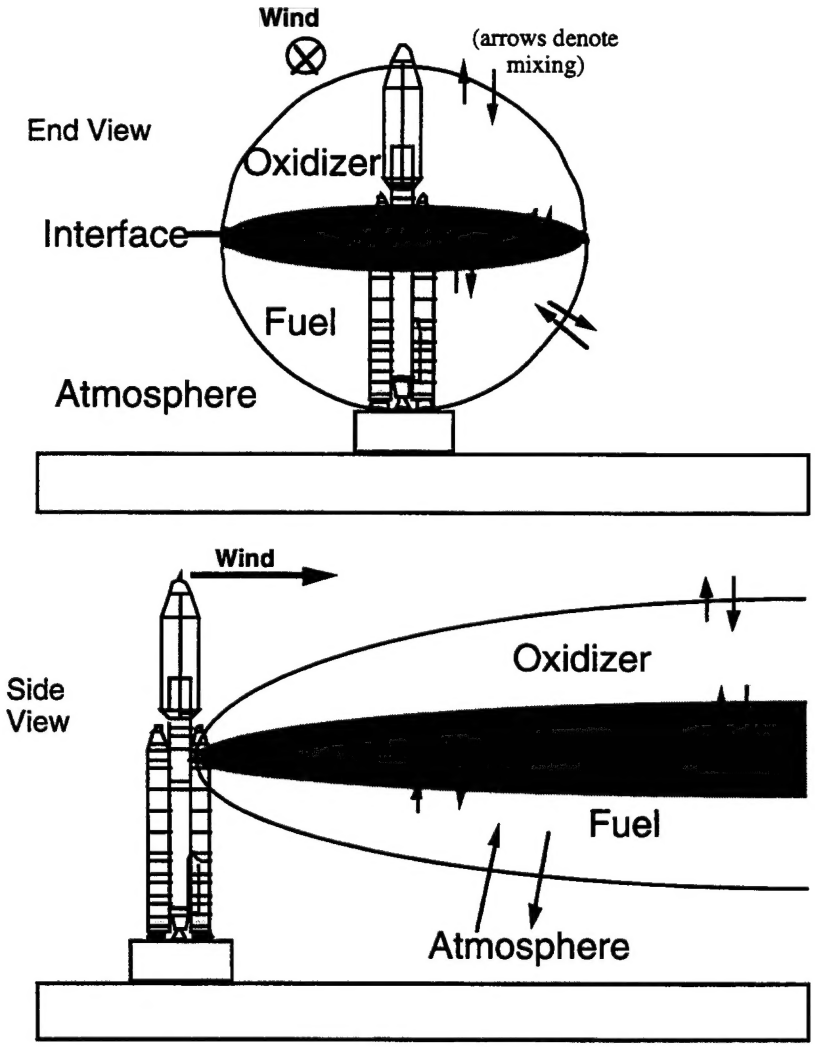

Figure 1. Topology of the four-bin model. Mixing takes place only between adjacent bins, as shown.

the same as for a single-bin plume mixing with the atmosphere. The total rate is divided between the fuel and oxidizer bins according to their relative size. Background atmospheric gas concentrations in the plume increase at the same rate that the plume gas concentrations decrease. Mixing between bins is assumed to occur at the same rate as mixing with the atmosphere. The rate of mixing between bins is an important variable for which we have no experimental data.

A separate set of initial conditions is used for the oxidizer bin, fuel bin, and atmosphere bin. The interface bin is a mixture of the fuel and oxidizer bins. The bins can vary in temperature and composition; the pressure is held constant at one atmosphere. The fuel bin is taken to be initially nearly pure hydrazine, N_2H_4, with a trace amount (0.01%) of helium (for tracking model dilution). Aerozine 50, the true rocket fuel, is 50% by weight 1,1-dimethyl hydrazine, UDMH. Addition of UDMH is treated in a later section. The oxidizer bin is initially assumed to be nearly pure NO_2 with a trace amount (0.01%) of argon. The propellants are assumed to be pure gas-phase initially to avoid the complication of treating multiple phases in the early stages of the abort. (Other phase combinations are treated in a later section.) We, therefore, assume a minimum temperature of 400 K for the propellant bins. This also forces the oxidizer to be completely dissociated to NO_2. Ignoring the vaporization of propellants and dissociation of N_2O_4 effectively adds heat to the plume. The amount of heat involved in vaporization and dissociation is small compared to the heat of reaction, but could be significant at early stages (see below). The rare gas mole fraction is always less than one percent and thus does not appreciably alter the density of the plume. The helium and argon do not participate in reactions. This allows us to test separately the effects of reaction and dilution in the various bins.

The background air is made up of nitrogen and oxygen in the usual abundances, 20 ppb nitrogen dioxide and water vapor varying with the humidity. The background air is also assumed to contain a marine aerosol (0.2 ppbv) 0.5 μm in diameter, and consisting of water and sodium chloride. Such an aerosol is typical at coastal sites, such as Cape Canaveral and Vandenberg Air Force Base. The proportions of water and salt in the aerosol vary with the humidity. All the cases modeled in this report were at 95% humidity. For computational simplicity, aerosol particles are also assumed to be present in the initial plume as well as in the atmosphere. The simulation was run at one atmosphere pressure and 293 K for a one-hour event.

The bulk-phase activity coefficients were set equal to the liquid mole fraction with two exceptions: water and nitric acid form an azeotrope, and the real activity coefficients for these species were fit to a quadratic equation in the mole fraction. This equation was used in the program. Thermodynamic data for the bulk species not available in SURFACE CHEMKIN were taken from the JANAF Thermochemical Tables (Chase[7]) and The International Critical Tables (National Research Council[11]). Surface species are assumed to have the same properties as bulk-phase species for this simulation. The temperature dependence of the gas phase rates is included.

The model was constructed to simulate the effects of a launch abort, within several seconds of ignition, of a large launch vehicle such as a Titan IV. Although the model described here was designed specifically to model the Titan IV, the results are also relevant to other vehicles that use hypergolic propellants such as Delta and Long March, and with minor adjustments, we could model those vehicles as accurately as the Titan IV. The Titan IV has three or four stages. The core vehicle is two stages using hypergolic propellant. The two fuel and two oxidizer tanks are stacked vertically,

alternating fuel and oxidizer, with the fuel on bottom and the oxidizer on top. The top of the core vehicle houses the stage-2 oxidizer (NTO); immediately below this is the stage-2 fuel (A-50). Below these are the somewhat larger stage-1 oxidizer tank(NTO), and the bottom-most tank is the stage-1 fuel tank (A-50). For simplicity, we have modeled this as one oxidizer tank atop one fuel tank. Separation into four tanks may provide somewhat better mixing. Beside the core vehicle are two strap-on solid motors using an aluminum/ammonium perchlorate propellant system commonly referred to as stage 0. We ignore the solids in the current problem; this is being left to future studies. A third stage may be carried on top of the core vehicle for some missions. The largest third stage uses liquid hydrogen and liquid oxygen, which are non-toxic if released. The third stage, if present, carries one-eighth or less of the propellant mass of the core vehicle. The satellite carries 2500 to 18,000 lb of hypergolic propellant, which is 0.6% to 4% of the propellant in the core vehicle. The satellite and optional third stage could potentially influence the heat balance and even the chemical composition of the abort cloud, but these effects are small with respect to the impact of the core vehicle and are ignored in the current study. A more in-depth study should include these effects.

The reaction mechanism includes 298 gas-phase reactions, eleven surface reactions, and two bulk-phase reactions. The reactions and rate constants are listed in the Appendix. Mass transport between phases is handled via surface reactions. Mass transport is assumed not to be rate limiting except for the case of reaction of N_2O_4 with the droplet surface, as discussed below. Using a formula for the characteristic time for macroscopic mass transport (interstitial gas-to-droplet diffusion) developed by Schwartz:[12,13]

$$(mt) = \left(12 D_g L \left\langle D^{-2} \right\rangle\right)^{-1},$$

where D_g is gas-phase diffusivity, L is liquid volume fraction, and D is the droplet diameter. For our calculated cloud properties, we get a characteristic time of about 0.1 s. Since the model results without mass transport limitation show that most of the aerosol chemical reactions take place on a scale of about 10 s, macroscopic mass transport should not be a limitation.

The rates of gas-surface reactions are put in as sticking coefficients, with all of these equal to 1 except that for the N_2O_4 + water reaction, which was varied from 1 to 10^{-3}, and 0 to "turn off" the heterogeneous chemistry. Recent experimental work on NO_2 indicates that the true sticking coefficient is substantial.[14] The surface-bulk reactions are put in as diffusion limited. The program tracks the concentration of each species in the plume, as well as the temperature, density, particle radius, surface-to-volume ratio, liquid-volume fraction, and time.

For the first 30 s of an abort, we use the four-bin model, but we do not allow any surface or condensed phase reactions other than simple condensation. The temperature of the cloud during this time is too hot to permit the existence of an aqueous phase. After 30 s, the separate bins of the plume are well mixed, and the cloud has cooled enough to condense water. For this later time period, we only use two bins to model the plume, but we include the full set of condensed and surface phase reactions (see two-bin results below).

A property of hydrazine that is important to the current problem is that it is a monopropellant. Pure hydrazine will decompose explosively if heated to 670 K. In our model, this decomposition occurs at 770 K (on a short time scale). We did not adjust any rates or temperature dependencies to achieve this agreement, merely using the literature values. While this agreement is not perfect, it is encouraging given the complexity of the mechanisms involved.

The decomposition of hydrazine points out some inadequacies in our model. We assume that each bin is at thermal equilibrium and can be represented by one temperature. The interface bin, where fuel and oxidizer are mixed, ignites rapidly, greatly increasing its temperature. Some of this heat spills into the adjacent fuel and oxidizer bins, but it is not enough heat to raise the entire fuel bin to 770 K, inducing decomposition. In a real fuel bin, however, thermal transfer rates are finite. There is a temperature distribution in the fuel bin. It would be hottest next to the interface and cooler farther away. It is thus possible that there is enough heat in the interface to set off an explosive decomposition of the nearest sliver of fuel. The exploding fuel would heat up and set off the next sliver of fuel, etc. We explored this possibility in two ways: we tested different sets of initial conditions, and we used a modified version of the program to model the fuel bin only. The first set of initial conditions involved raising the temperature of the fuel bin, while leaving other parameters unchanged. We explored seven initial fuel temperatures from 400 K to 800 K. The second set of initial conditions varied the size of the fuel bin relative to the interface bin; the oxidizer bin was kept at the same size as the fuel bin. We used five different fuel-to-interface volume ratios from 16:1 to 1:10. The largest value corresponds to premixing 3% of the propellant; this is in agreement with the values arrived at in the Lockheed Martin report.[1] The smallest values used correspond to an attempt to model only the sliver of fuel nearest to the interface bin. We used the full set of starting fuel temperatures for each fuel-to-interface volume ratio, giving a matrix of 35 data sets. We also did a set of tests where we varied the stoichiometry at a single initial fuel temperature and fuel-to-interface ratio. In our second approach, we modified the program to model the fuel tank as three bins. The first bin was started at 800 K so it would ignite, the next bins were cooler, and the final bin mixed with the atmosphere. The volume ratio of the three fuel bins was also varied.

4. Multi-Bin Results

4.1 A Typical Run

Figures 2–4 show the species concentrations and temperatures in the three plume bins for a typical model run. The case shown here is for an initial fuel temperature of 700 K and a fuel bin to interface ratio of 1.6 to 1 (this ratio initially gives 23% of the propellant consumed to agree with the LMC report). Figure 4 shows the interface bin, which ignites a little after a tenth of a second. The fuel and oxidizer are consumed rapidly, the temperature shoots up to about 3000 K, and product species such as water begin to dominate. The fuel bin (Figure 2) ignites after a little more than half a second, a delay of 0.4 s from the interface bin ignition. The temperature does not get as high in the fuel bin, falling just under 2000 K. There is little oxidizer in the fuel bin, but the fuel is consumed on ignition. The quick rise in hydrogen suggests that most of the hydrazine is converted to hydrogen and nitrogen; the amount of ammonia formed is an order of magnitude less. The oxygen concentration, which was

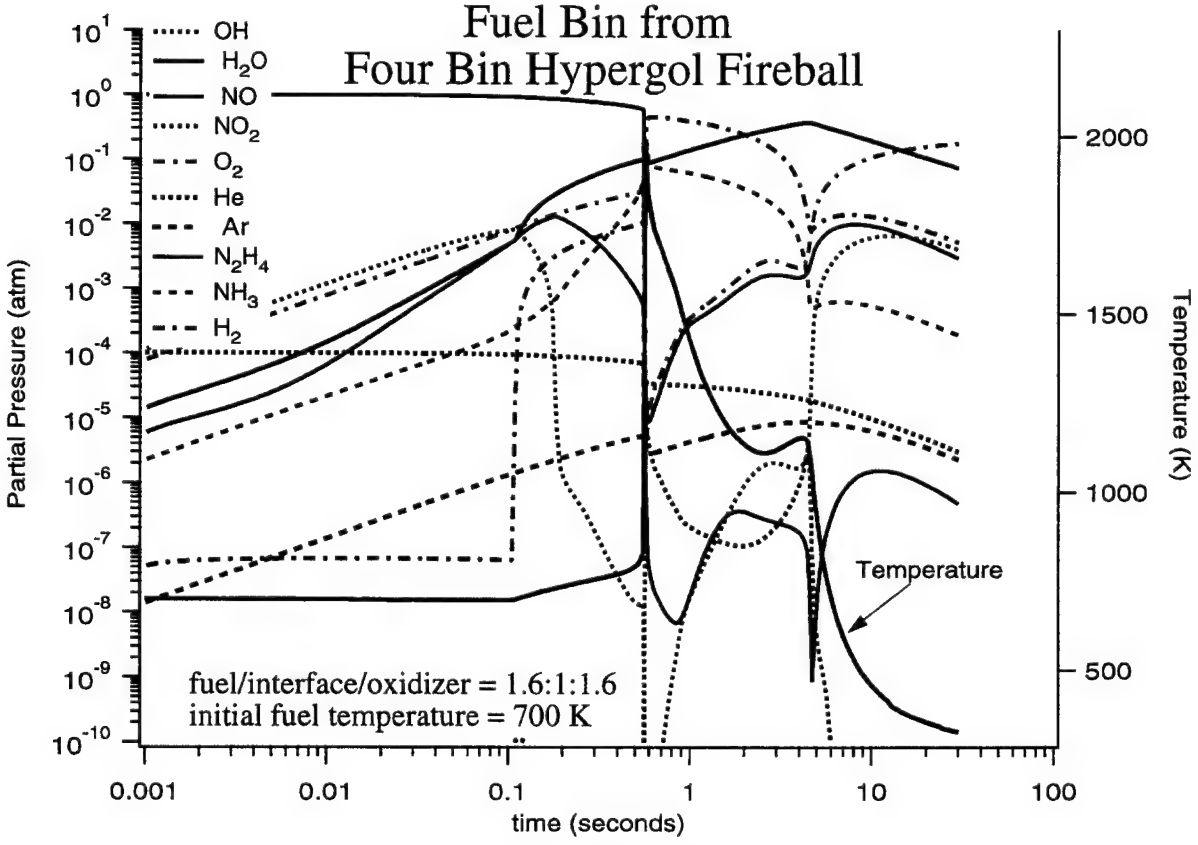

Figure 2. Time dependence of the major species concentrations in the fuel bin. Initial bin temperature is 700 K. Ratio of fuel bin to interface bin volumes is 1.6 to 1.

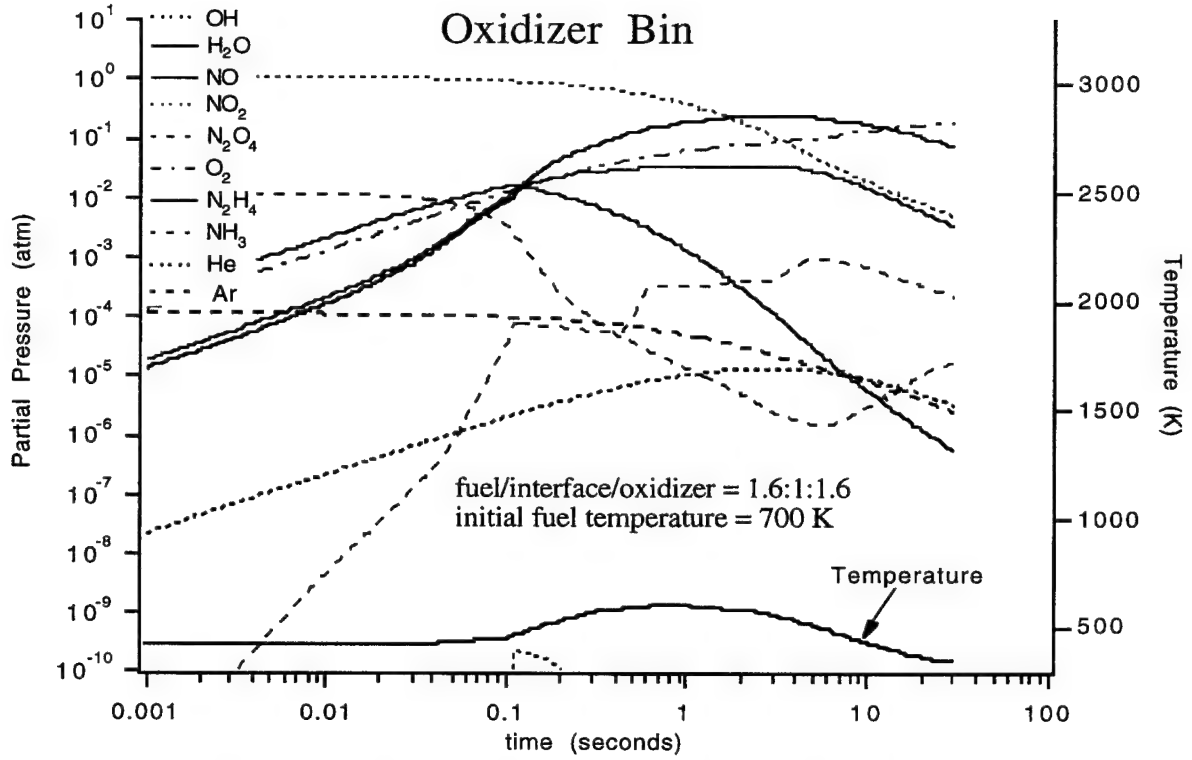

Figure 3. Conditions as in Figure 2, concentrations of species in the oxidizer bin.

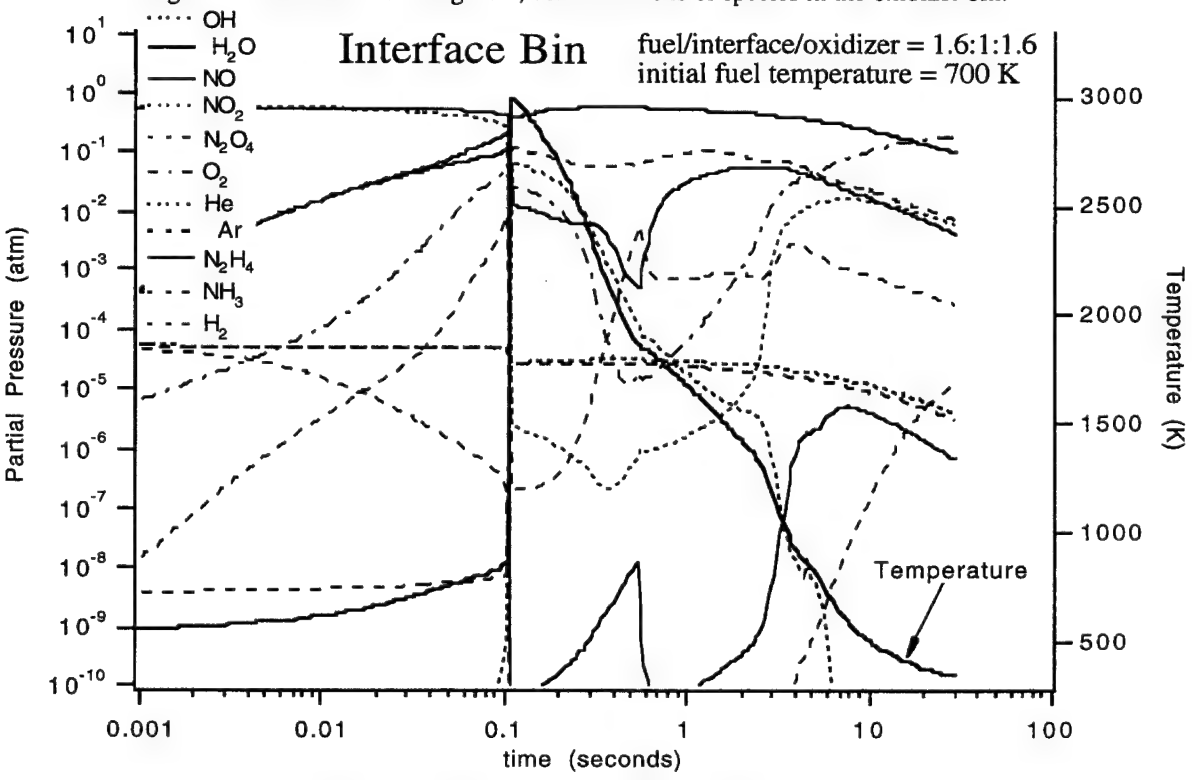

Figure 4. Conditions as in Figure 2, concentrations of species in the interface bin.

rising due to mixing with the air, is also depleted upon ignition, and doesn't begin to rise again until the hydrogen is consumed. At this point, the water concentration begins falling. This suggests that the hydrazine undergoes unimolecular decomposition, and the hot hydrogen product burns with oxygen as fast as it is mixed in. In contrast to the first two bins, the oxidizer bin is relatively quiet. The temperature and species concentrations do not change dramatically over the timescale of the simulation.

4.2 Summary of Results on Bin Size and Temperature

4.2.1 Ignition Delay Studies

As described earlier, one of our first concerns was to determine whether the fuel bin ignites. Ignition of the fuel bin will have a large impact on the plume because it destroys hydrazine, which is then unavailable to react with and neutralize the nitrogen oxide oxidizer, or to be a toxic hazard downstream. In addition, ignition of the fuel bin will release additional heat into the plume. This heat will contribute to the buoyancy of the plume, lifting the toxic cloud off the ground and away from people. The results of our tests with variable bin size and starting temperature are shown in Figure 5. The reciprocal of the ignition time is plotted against temperature (x axis) and fuel-to-interface ratio (y axis). The value of 27 s^{-1} (37 ms) (white) corresponds to the shortest ignition time or most easily ignited fuel bin. The value of 0 s^{-1} (black) corresponds to a fuel bin that does not ignite. It is obvious that higher initial temperatures and smaller slices of the fuel bin correlate with faster ignition.

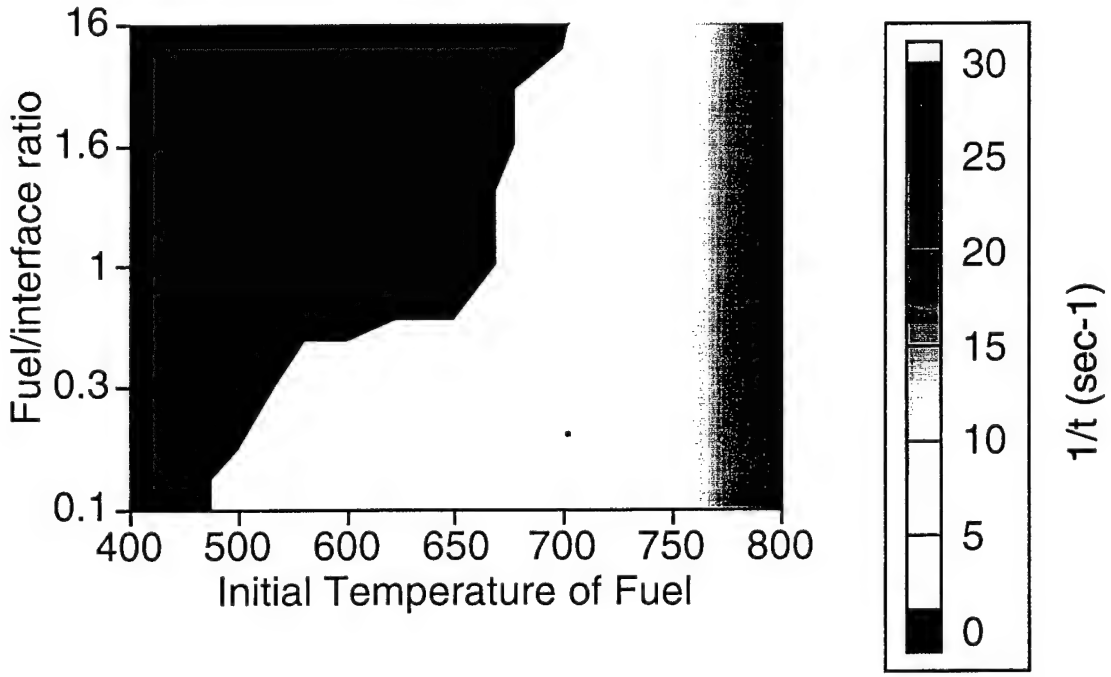

Figure 5. Contour plot of the reciprocal time to ignition as a function of initial bin temperature and fuel-to-interface volume ratio. Red areas ignite quickly; black areas do not ignite.

We also modified the model slightly to model just the fuel tank and the atmosphere as described in the previous section. The bin closest to the interface always ignited because we started it off at 800 K. The adjacent bins ignition depended on several factors, one of which was relative bin size; under no conditions would the adjacent bin ignite if it was the same size or larger. How much smaller the adjacent bin had to be depended on initial temperature. This would indicate that while some of the fuel tank is ignited, and that ignition spreads to some adjacent sections, the entire fuel load will not be consumed in this way. The exact fraction of the fuel load that burns as a monopropellant will depend on the mixing rates, the geometry of the abort, and the energy available from other sources, such as the solids.

We did only one test of the dependence on stoichiometry. Starting at a temperature of 700 K and a fuel bin to interface ratio of 1.6, we varied the stoichiometry from 0.75 (lean) to 1.25 (rich). The lower the fuel-to-oxidizer ratio, the more likely the fuel bin was to ignite. Actual launch vehicles are 10 to 12% fuel rich. The lower boiling point of the oxidizer may favor a lean mixture in the gas phase. The stoichiometry of the interface region will also depend strongly on the geometry of the breakup.

4.2.2 High-Temperature Destruction of NO_x

There is a great deal of interest in the amount of conversion of nitrogen oxides to nitrogen and oxygen at high temperatures. We did some studies with high initial temperatures to learn about this. The model results show that at initial plume temperatures above 298 K, but below 3000 K, we observe behavior that is best described as evolutionary from that seen at 298 K. If we start at $T^0 = 1500$ K, for example, essentially all of the N_2O_4 is dissociated, and even some of the NO_2 is decomposed to give NO. This results in substantial cooling of the plume to 800 K. The plume then cools until it reaches approximately 373 K, at which point the nitric acid and water again condense. Careful accounting shows that the majority of the NO_x is still present in the aerosol as nitric acid. However, about 9% is destroyed by thermal decomposition. These results are typical of the range $T^0 = 300–3000$ K. They suggest that if the plume comes in contact with the ground, deposition of the aerosol to the ground should be considered as a significant NO_x loss mechanism from the plume.

The behavior observed at $T^0 = 3000$ K is markedly different from that observed at lower temperatures. Within the first 0.1 s, a rapid temperature rise appears accompanied by a sharp reduction in NO concentration. This is the result of NO_x conversion to N_2 and O_2. The high T^0 leads to the rapid initial decomposition of N_2O_4 all the way to NO. The combination of high temperatures and high NO concentration permits the chemical decomposition of NO. The presence of N_2O and its correlation with NO loss confirms this process for destroying NO_x. A minimum sustained temperature of >2000 K is necessary for this process to become efficient. In this case, >95% of the NO_x is destroyed. Since most of the NO_x is destroyed within the first second, there is little aerosol formation. This is clear from the peak aerosol radius, which is an order of magnitude smaller than observed at $T^0 = 298$ K.

To summarize: from ambient temperature to 1000 K, the NO_x loss rises from zero to approximately 9%. Over a broad temperature range, 1000–3000 K, the NO_x destruction is largely constant at about 9%. Above 3000 K, the NO_x destruction cycle discussed above becomes important, and essentially all of the NO_x is destroyed.

4.2.3 Residual NO_x and Hydrazine

Figures 6 and 7 show the residual NO_x and hydrazine after 30 s under the same conditions as Figure 4. The residual toxic gases are plotted as a fraction of the initial amount (the total fuel or oxidizer on the vehicle) vs. the fuel-to-interface ratio; different initial temperatures are plotted on the same graph with different symbols. For the smaller bin ratios, the amount of propellant remaining is not the total, but only that in the sliver next to the interface region, since the entire propellant tank was not modeled. It is obvious from Figures 5–7 that ignition of the fuel bin greatly reduces residual hydrazine, but the dependence of residual NO_x on initial temperature is more complicated. The highest bin ratio shows the greatest amount of residual toxic gases, which is in fair agreement with previous reports. These figures illustrate the difficulty of "averaging" the results of different scenarios.

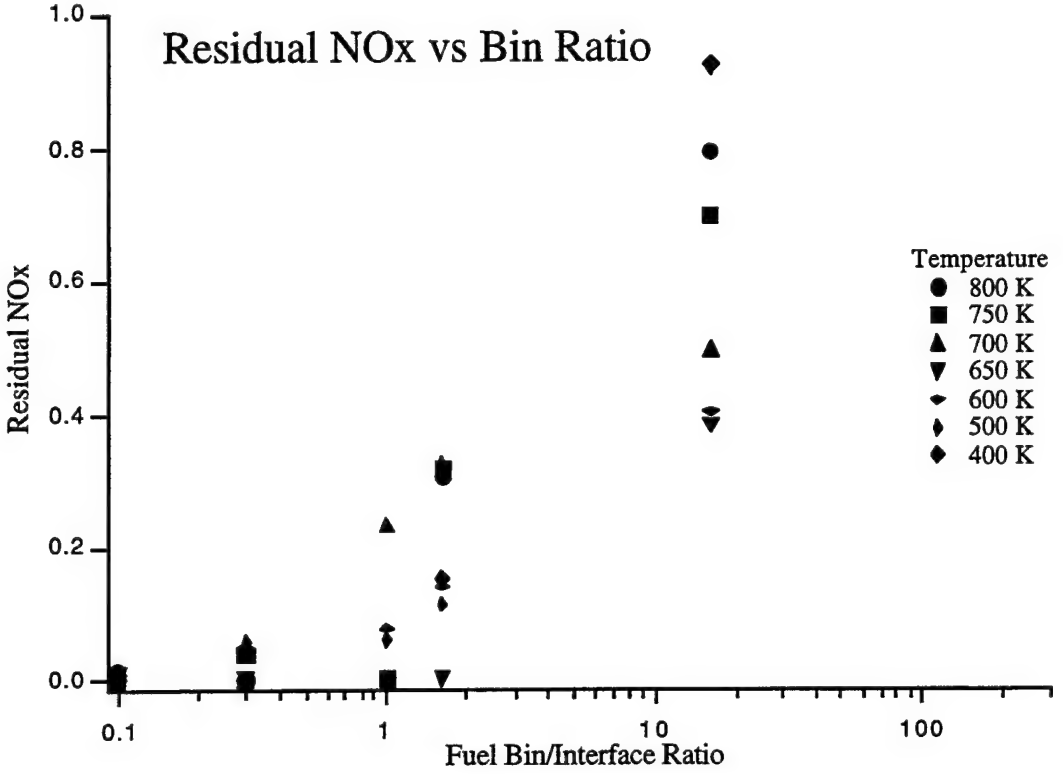

Figure 6. Residual NO_x as a function of initial temperature and bin volume ratio. All points are at 30 s.

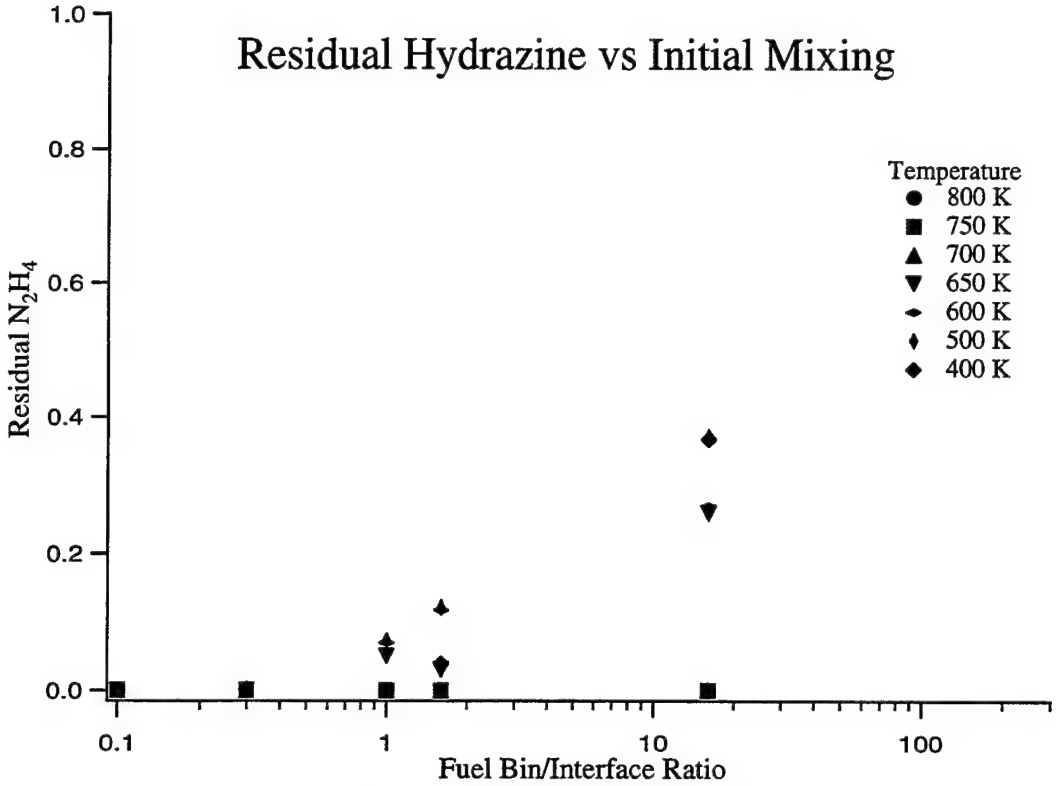

Figure 7. Residual hydrazine at 30 s.

5. Additional Two-Bin Studies

In the multi-bin version of the model described above, some simplifications were made in order to get quick results. In the work described in this section, we explore the consequences of those simplifications by means of two-bin calculations.

First, in the multi-bin model, we ended the calculations at 30 s in order to avoid dealing with the heterogeneous chemistry of nitrogen oxides that begins as the plume cools to near ambient temperatures. After 30 s, this liquid-phase chemistry begins to convert the nitrogen oxides to nitric acid, as was seen in our cold spill studies.[3] Inclusion of this was examined by taking the multi-bin results at 20 s and re-initializing a two-bin calculation at that time. The results will be discussed below.

Second, we always started with gaseous fuel and oxidizer. This kept the chemistry all in one phase, and speeded up the computations significantly. However, this restriction required that the initial temperature for the event had to be above 400 K so that the hydrazine would all be evaporated. In a real abort, some of the fuel is almost certainly initially in the liquid phase because of its rather high boiling point. We have now included in the model a two-phase fuel bin to permit low starting temperatures. The results are discussed below.

Third, we also simplified the chemistry in the initial version by including only hydrazine, N_2H_4, in the fuel bin. The actual fuel is Aerozine-50, which is 50% hydrazine and 50% unsymmetrical dimethyl hydrazine, $(CH_3)_2N_2H_2$. We included the UDMH chemistry in some two-bin calculations as described below.

5.1 Extension to Longer Times with Heterogeneous Chemistry

In order to include the aerosol chemistry, we take the results obtained from the four-bin model at 20 s and use them as the starting conditions in a two-bin heterogeneous run that extends to one hour. Application of the two-bin model is possible because the gas concentrations in the initial three bins tends to converge at 20 s (see Figures 2–4), and there is no liquid-phase formation until after this time. The results of the 1.6 fuel-to-interface ratio case are shown in Figure 8. We still see about 50% conversion of the NO_x to nitric acid. Figure 9 summarizes several runs and shows that including heterogeneous chemistry and following the plume for an hour after the abort results in less (13–20%) residual NO_x ($NO + NO_2$) for low initial temperatures. For initial temperatures above 650 K, there is an increase in NO_x (solid squares) and the additional formation of nitric acid (solid triangles). This is results because the hydrazine fuel spontaneously decomposes above this temperature, and therefore there is less available to "titrate" the oxidizer. The higher resulting residual oxidizer tends to form more nitric acid.

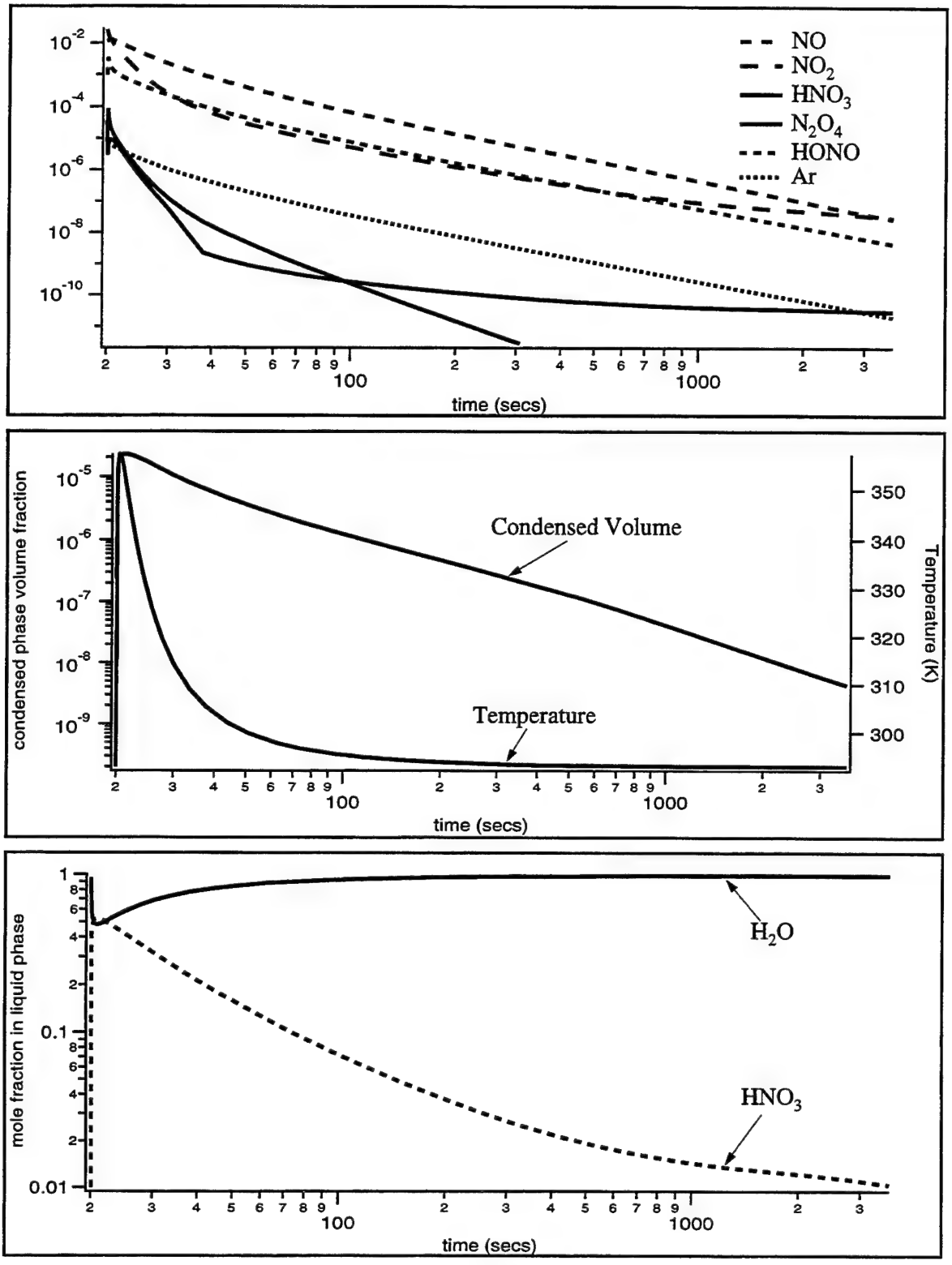

Figure 8. Results of 2-bin continuation model from 30 s to 1 h. ($t^0 = 20$ s).

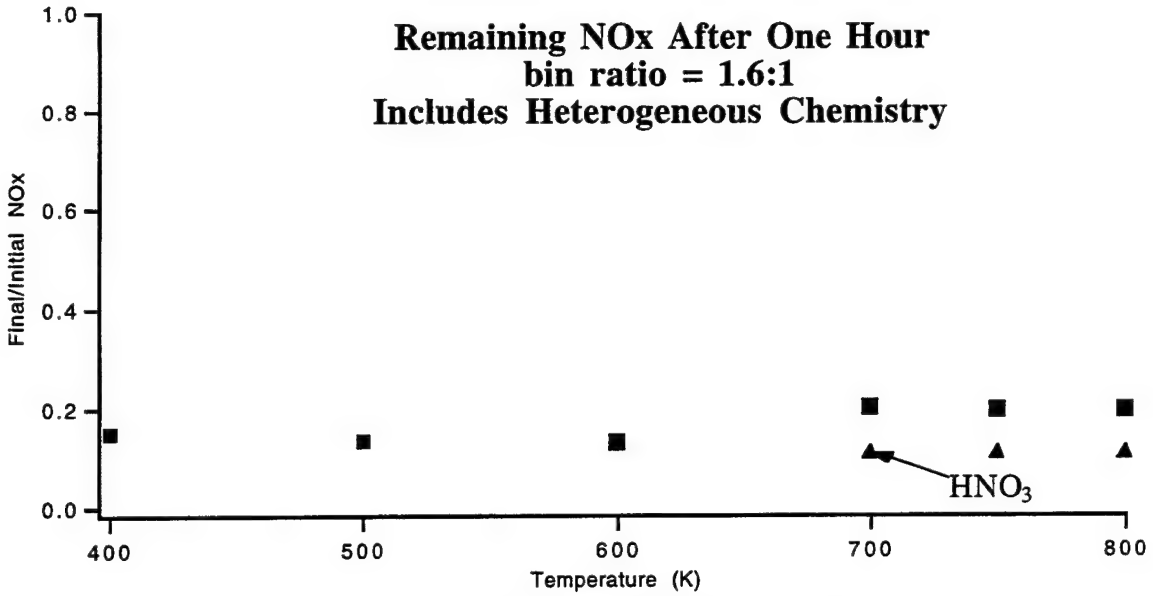

Figure 9. Summary of remaining NO_x ($NO + NO_2$) in gas phase for various initial temperatures at 1 h, including heterogeneous chemistry.

5.2 Fuel Initially In Liquid State

The liquid fuel results were tried in a two-bin model to see what happens in a simplified system. These results are shown in Figures 10–15. Runs are shown for the four possible combinations of gaseous and liquid hydrazine and dissociated and undissociated nitrogen tetroxide. Figures 10–13 show species. Figures 14 and 15 show temperature histories.

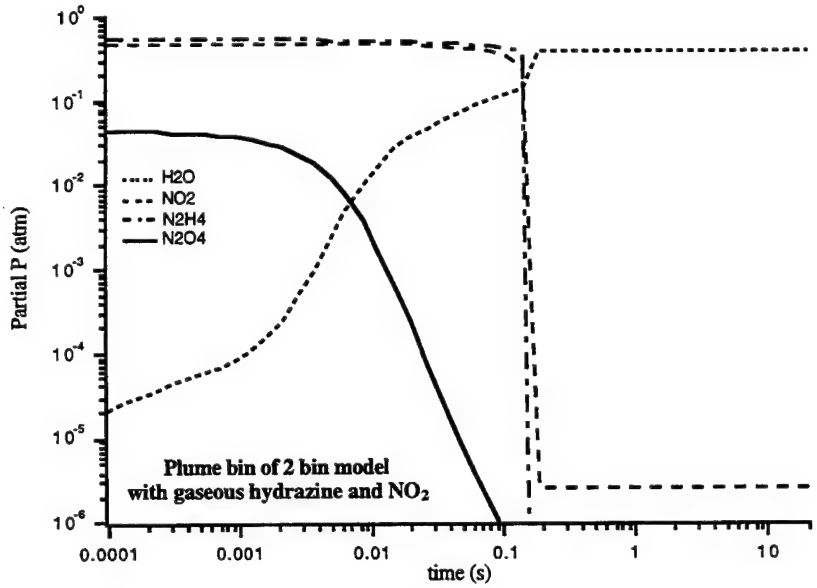

Figure 10. Two-bin results for N_2H_4 (g)/NO_2 (g).

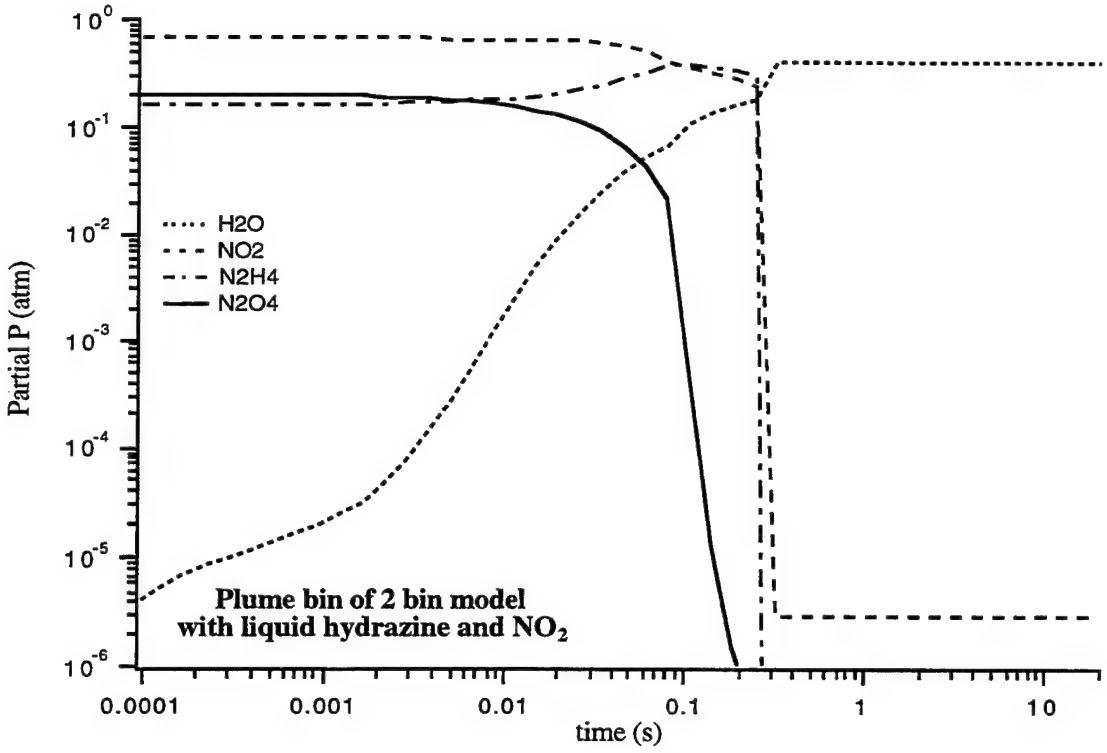

Figure 11. Two-bin results for N_2H_4(l)/NO_2 (g)

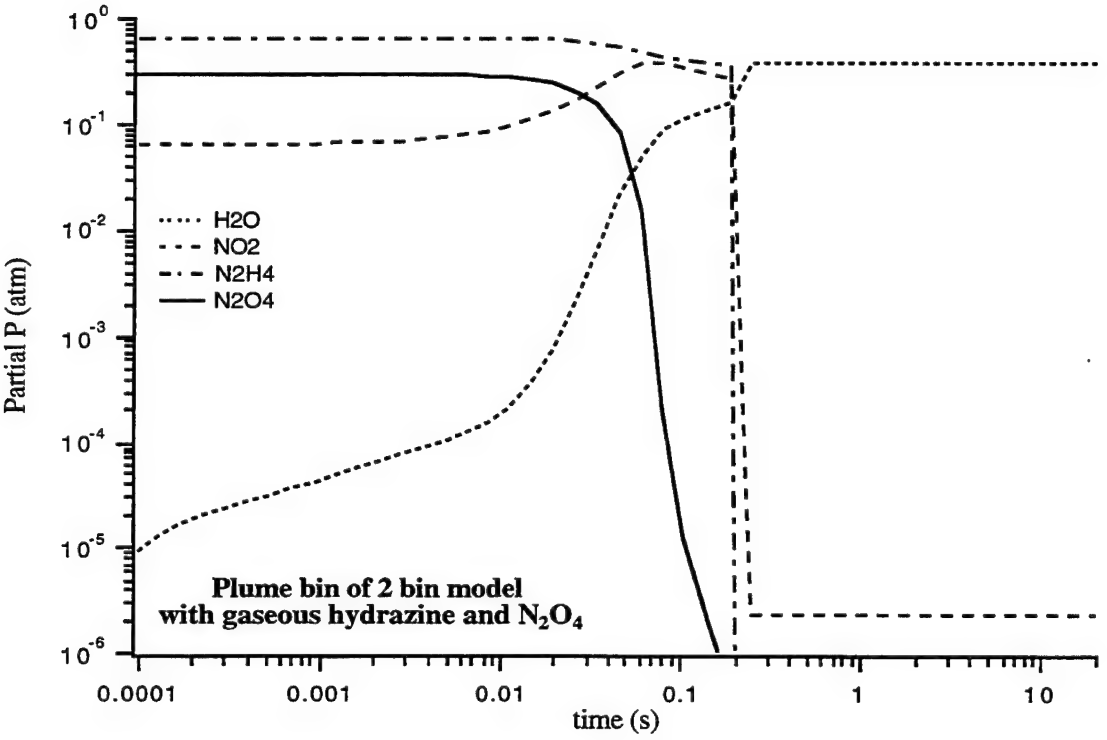

Figure 12. Two-bin results for N_2H_4(g)/N_2O_4 (g)

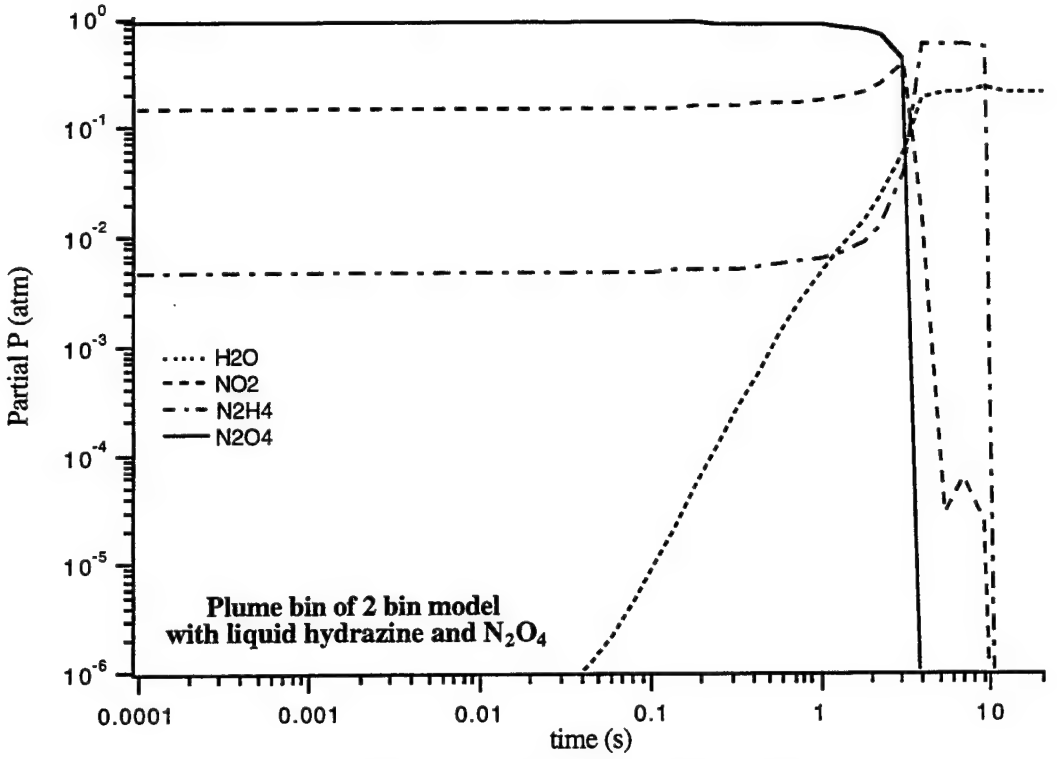

Figure 13. Two-bin results for N_2H_4 (l)/N_2O_4(g).

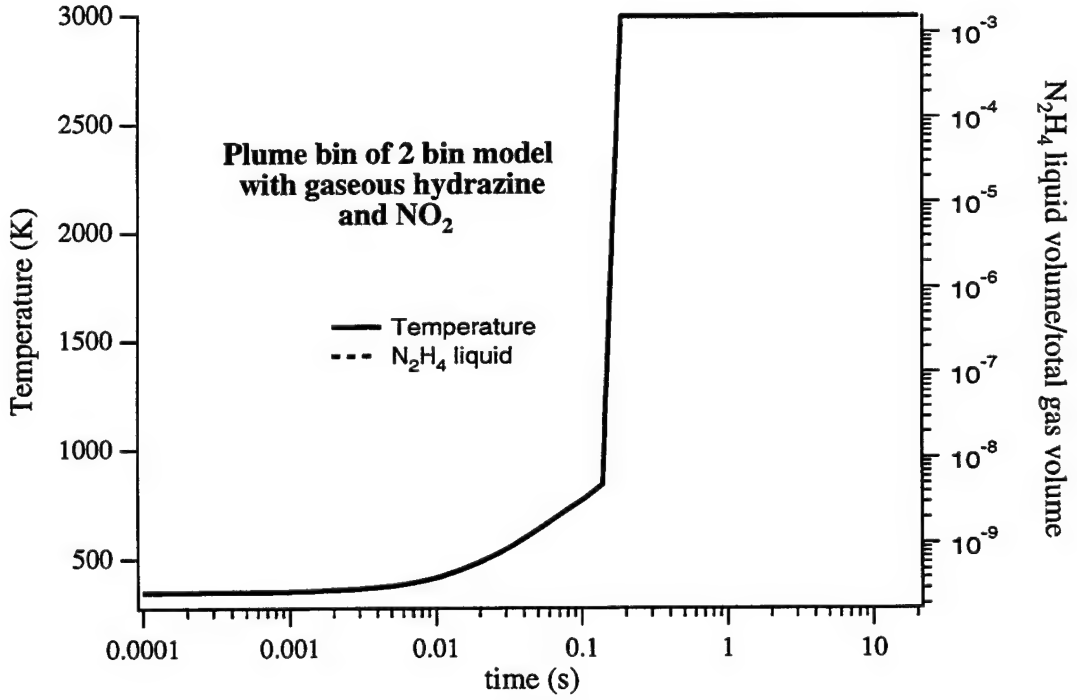

Figure 14. Two-bin results for N_2H_4 (g)/NO_2 (g). Temperature history for Fig. 10.

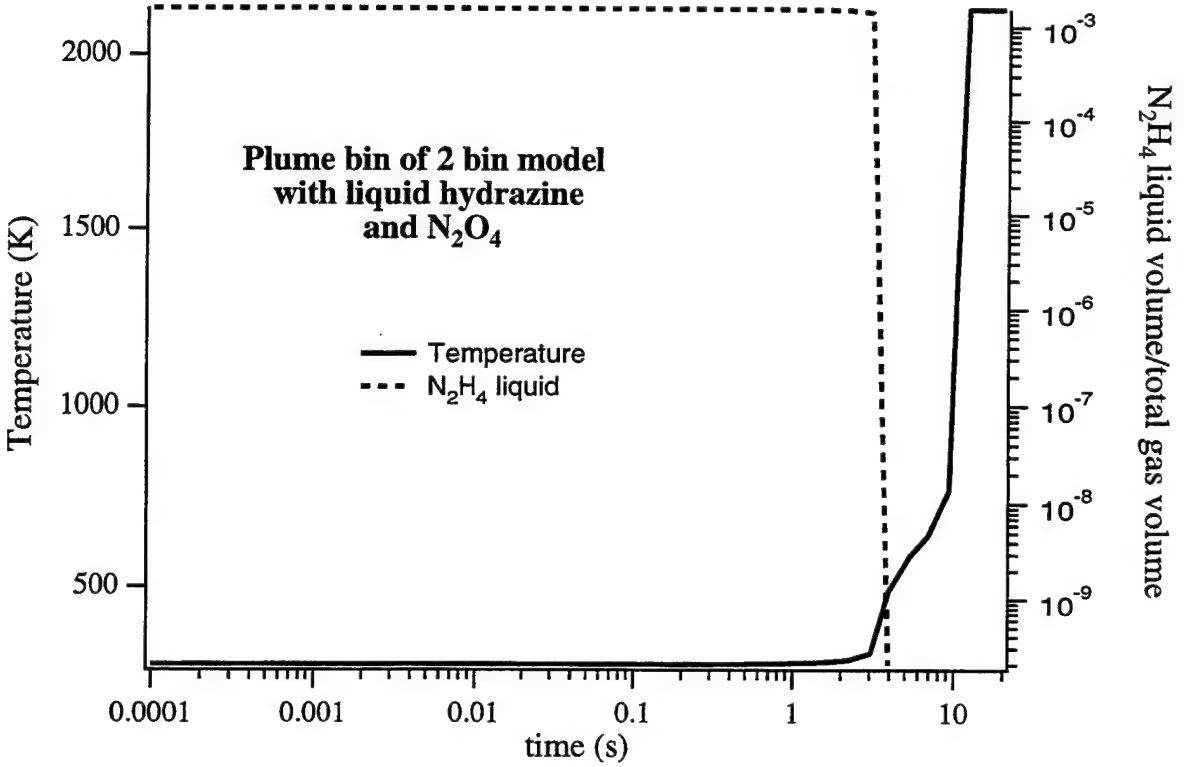

Figure 15. Two-bin results for N_2H_4 (l)/N_2O_4(g). Temperature and phase profile for Fig. 13.

Since water is a reaction product, it is an indicator of how the oxidation of hydrazine is proceeding. Note that in the liquid hydrazine runs, the hydrazine partial pressure is low initially, and then rises as the system heats up and raises the vapor pressure of the liquid. The "plateau" in the hydrazine pressure occurs when all of the liquid has evaporated. Finally, combustion destroys all the hydrazine, and its partial pressure falls at about 10 s into the event. Note that the peak temperature is considerably lower in Figure 15, and the onset of ignition is delayed from a few tenths of a second to a few seconds. This is seen only for this case (liquid hydrazine and undissociated nitrogen tetroxide). Nevertheless, this case is the most likely initial condition in our view. If these two-bin results are typical, then the peak temperatures are considerably lower (2200 K vs 3000 K), and the overall chemistry may be different. Table 1 summarizes the residual gases for the four cases studied. There is a small increase in NO_x and ammonia for the "coolest" case.

Table 1. Residual Gases vs. State of Reactants

	NO_x	N_2H_4	NH_3/N_2H_4
N_2H_4(g)/NO_2(g)	4.90%	<0.00%	<0.00%
N_2H_4(g)/N_2O_4(g)	4.54%	<0.00%	<0.00%
N_2H_4(l)/NO_2(g)	4.80%	<0.00%	<0.00%
N_2H_4(l)/N_2O_4(g)	5.67%	<0.00%	3.19%

5.3 Inclusion of UDMH Chemistry

Including UDMH chemistry in the reaction manifold requires a great deal of additional information. First, we must propose a combustion mechanism for that molecule; second, we must estimate thermodynamic properties of many of the intermediate species; third, we must estimate rate constants for all the reactions. The combustion mechanism is based on the atmospheric chemistry results for UDMH obtained at Riverside.[2]

A full UDMH reaction mechanism was constructed by combining the hydrazine (used in the multi-bin model) and standard methane[6] reaction mechanisms. Additional chemistry was then added to account for the first degradation steps of UDMH. The previous studies of the atmospheric degradation of UDMH provided the basic set of reactions. Reaction channels open only at high temperature were then added, including hydrogen abstraction reactions by hydroxyl radicals and unimolecular decomposition of UDMH and its decomposition products. Where available, literature values for the rate constants were used. Missing rates were estimated based on analogies to similar rates in hydrazine and methylamine chemistry.

The thermodynamic data for the UDMH model were taken from the JANAF tables[7] where available. Many of the species were not present in the tables, and their thermodynamic properties had to be estimated. For this purpose, we used the MOPAC 6 semi-empirical chemistry package.[15] MOPAC calculates the molecular energies, geometries, and force fields using a combination of molecular orbital theory with empirical corrections to facilitate rapid computation. MOPAC then uses statistical mechanics to calculate the thermodynamic properties required by CHEMKIN. Due to the inherent limitations of semi-empirical methods, the absolute energies are often in error by several kcal/mole; however, the relative energies and geometries from these calculations are typically much more accurate. Thus, where possible, we have substituted other more accurate measured or calculated values for the heat of formation at 298 K. The data sources are summarized in Table 2. The complete mechanism is given in the Appendix.

Table 2. Species with MOPAC estimated thermodynamics.

Species	Used literature ΔH298
$(CH_3)_2NNH_2$	x
$CH_2CH_3NNH_2$	
$(CH_3)_2NNH$	
$(CH_3)_2NN$	
$(CH_3)_2NNNN(CH_3)_2$	
$(CH_3)_2NNHO$	
$(CH_3)_2NNO$	
$(CH_3)_2N$	x
$(CH_3)_3N$	x
CH_3NCH_2	

The two-bin results using the full Aerozine-50 chemical mechanism are shown in Figures 16 and 17. Significantly, the time profiles show an earlier formation of products than the pure hydrazine results do, which is in accord with the lower experimental decomposition temperature of UDMH relative to hydrazine. Our most recent work on the UDMH problem shows that HCN is an important pyrolysis product, and we need to include reactions leading to the formation of this very toxic product in the future.

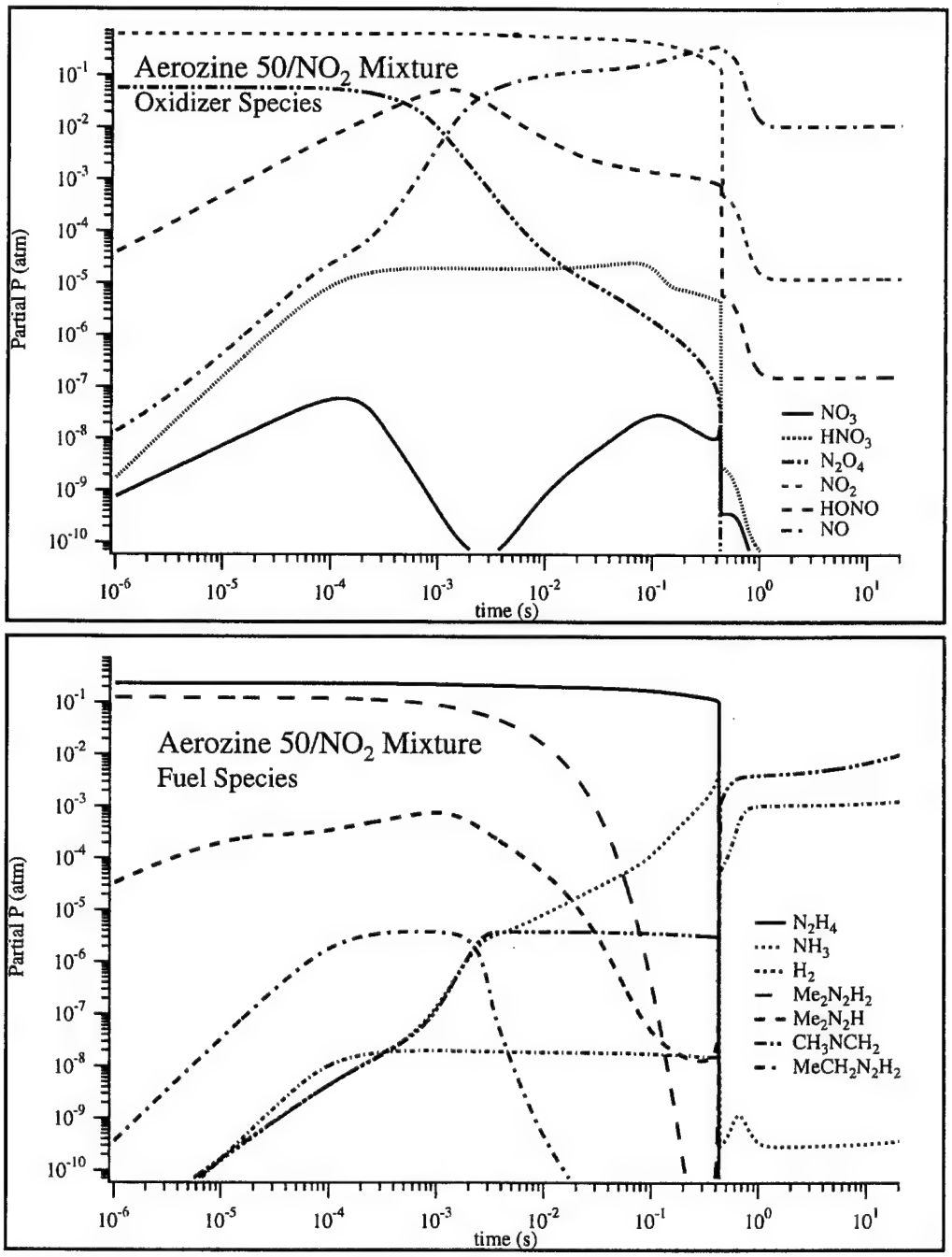

Figure 16. Two-bin results for UDMH. Fuel and oxidizer species.

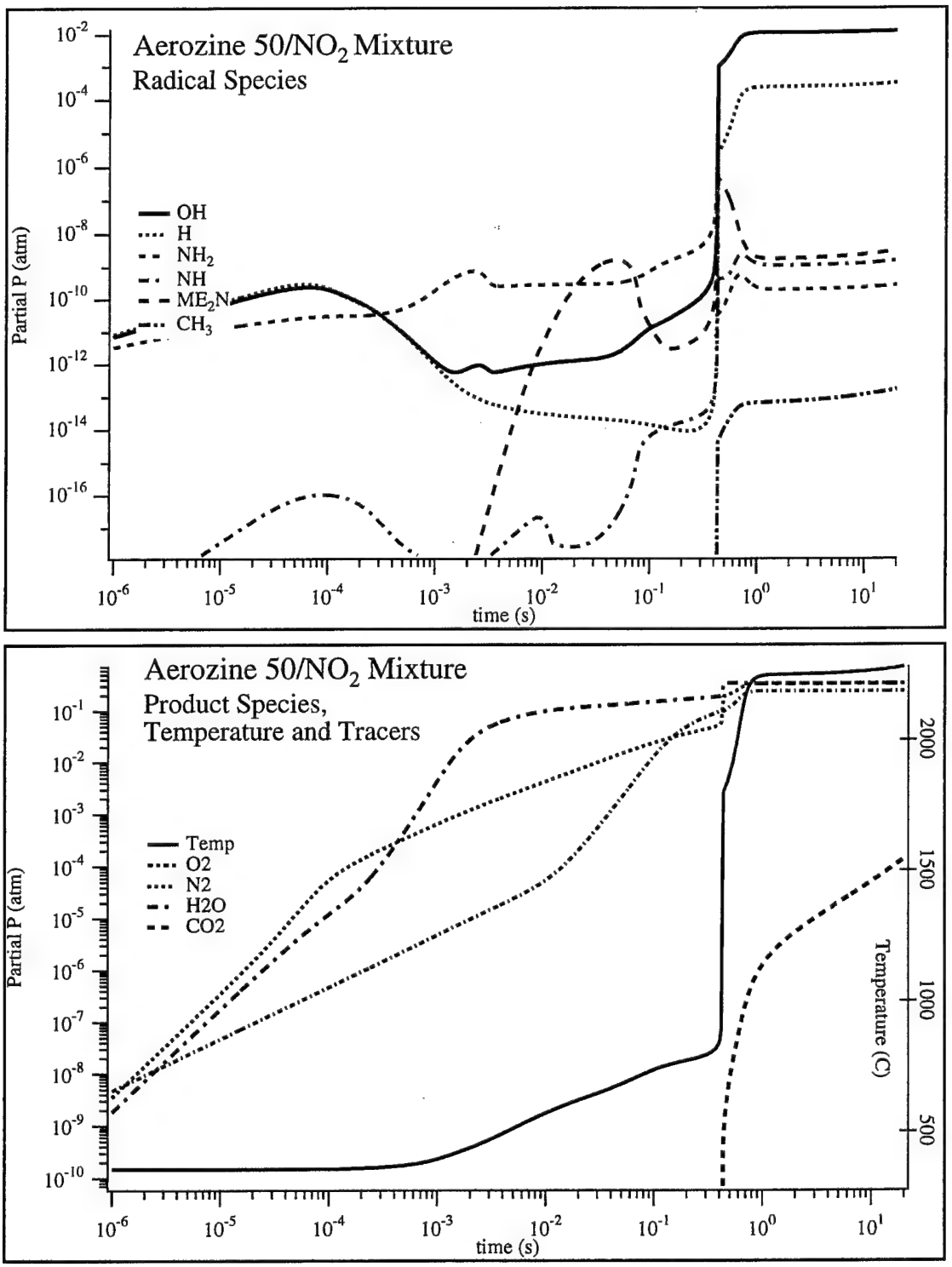

Figure 17. Two-bin results for UDMH. Radical species and temperature history.

6. Comparison with the Thermodynamic Model Results

In discussing our comparison to the Lockheed-Martin (L-M) report in detail, we will begin with the fireball temperature distribution.

The core temperature and outside temperature of the fireball are the same in the L-M report[1] and in our report. The core temperature is 3000 K (but see two-bin results with fuel initially in the liquid state), and the outside is the same temperature as the ambient air. The L-M report assumes that the temperature drops linearly from the core to the outside edge of the fireball. Our model has limited spatial resolution, but it does allow us to say something about the temperature distribution. The temperature drop is much faster than linear. In all of our runs, the core temperature reached 3000 K, but in none of our runs did the temperature of the adjacent oxidizer bin rise above 600 K; from there it is a small drop to the ambient temperature of 300 K. This appears to be due to the large heat capacity and endothermic reactions of the oxidizer. The temperature drop also appears to be non-symmetric; the temperature falls more slowly on the fuel bin side of the fireball. In nearly all our runs, the sliver of the fuel bin closest to the interface reaches 1800 K. How fast the temperature drops from here to the ambient temperature at the edge of the fireball depends on the amount of fuel that ignites as a monopropellant. The amount of fuel that burns in this way depends critically on the assumed conditions and cannot be predicted with accuracy. Nevertheless, it appears that even on the fuel side, the temperature drop is likely to be faster than linear.

Table 3 compares some of our results with those in the L-M report (taken from page 102, Table 31 in Ref. 1.). In Table 3, the percentages are mole percentages of the separate fuel or oxidizer. For both cases, the mole percentages are referred to atomic nitrogen. For the oxidizer, the percentages will be roughly a factor of 2 higher than the convention used in the L-M report, which is given as a percentage of the total initial load of fuel + oxidizer. For the fuels and the ammonia, the percentages are based on the hydrazine and UDMH taken separately, and these will be four times higher than the convention in the L-M table.

Table 3. Major Emissions (% of Fuel and Oxidizer Load)

Species	L-M Report	400 K 30 s	700 K 30 s	400 K 1 h	700 K 1 h
NO_2	44.02	0.00	18.84	0	1.08
NO	.80	15.27	13.34	14.05	16.85
HONO		0.83	2.22	1.37	2.39
HNO_3	5.34	0.07	0.10	0.00	0.02
HNO_3(l)				0.48	12.58
Total NOx	**50.16**	**16.17**	**34.51**	**15.90**	**32.91**
N_2H_4	4.87	3.91	0.02	3.80	0.00
UDMH	24.26				
NH_3	38.03	0.00	0.65	0.00	0.66

The L-M report assumes that 2–3% of the propellants are mixed initially, and that 23% of the propellants burn hypergolically. Our model does not include the turbulent fluid dynamics necessary to model the short time mixing. Therefore, we believe that our fuel-to-interface ratio of 1.6:1, which represents 23% of the propellant mixing initially, is the best match to the L-M data. In this case, we see 67–100% of the NO_2 oxidizer destroyed, which is significantly more than the 50% seen in the L-M report (see Figure 6).

The hydrazine fuel may be destroyed by burning as a bipropellant or as a monopropellant, so 98–100% of the fuel is burned. The more the fuel burns as a monopropellant, the less is available to burn with oxidizer, and the more oxidizer remains. The L-M report also indicated that 94% of the fuel would burn as a monopropellant, but they did not indicate the consequences this had for residual oxidizer. The L-M report found that hydrogen generated by fuel decomposition would burn with oxidizer; we find the hydrogen burns with air, leaving more oxidizer unreacted. Afterburning with air was expected by L-M researchers, but they assumed it would occur after the fuel and oxidizer reactions, and so they left it out of the fireball chemistry.

The L-M report finds that 35% of the oxidizer thermally decomposes. We find negligible thermal decomposition of oxidizer (5–10%) but we find substantial conversion to nitric acid: 25–50% of what survives the initial fireball. The L-M report did not consider nitric acid conversion. Our previous studies found larger conversion efficiencies to nitric acid (>90%) for cold oxidizer spills. The lower conversion seen here is due to the higher starting temperature and dissociation of much of the N_2O_4 to NO_2, and the lower concentration of NO_2 due to destruction by reaction with hydrazine.

7. Conclusions

7.1 General

The general conclusions are that, compared to the Lockheed-Martin (L-M) thermodynamic model, our model gives lower (and very brief duration) average fireball temperatures, more HNO_3, and much less NH_3. If we "average" the results of a number of runs with different starting temperatures, we get the following results.

- About 24% of the initial oxidizer remaining and 2% of the initial fuel remaining. These are roughly half the values from the L-M report (see Table 3, averaging the 400 K and 700K initial temperatures). The value for remaining oxidizer presently used in REEDM is 70%, which is a composite of the L-M fireball assumptions and our thermal decomposition numbers.

Additional conclusions from the two-bin studies are:

- Extension of results to 1 h with heterogeneous chemistry gives about 40% conversion of the NO_x to nitric acid. Higher amounts of initial NO_x give higher percentage conversions to nitric acid and vice-versa (see below).

- Starting with liquid N_2H_4 and undissociated N_2O_4 instead of the gaseous species delays ignition and lowers peak temperatures, but does not substantially change NO_x.

- Including UDMH in the reaction mechanism requires 300 reactions. The runs do not indicate any substantial changes in residual fuel or NO_x, but some new toxic materials are present, such as dimethylnitrosamine and HCN.

As previously stated, the amount of NO_2 converted to nitric acid depends on many other aspects of the problem; the more NO_2 is destroyed by burning with hydrazine or by thermal decomposition, the less will be converted to nitric acid. Because the acid conversion is second order in NO_2 concentration, the trade-off between conversion efficiency and other destruction pathways is not linear. Thus, it is problematic to find an acid conversion efficiency that can be meaningfully compared with the thermodynamic model, which does not include heterogeneous chemistry. The current REEDM model assumes that 23% of the original oxidizer amount is destroyed by hypergolic reaction with hydrazine, and 7% decomposes thermally. If we adjust the output of our four bin model to reflect these assumptions, and then run the two-bin follow-on model, we find that 32.5% of the original oxidizer (i.e., 50% of the residual oxidizer) is converted to nitric acid. Therefore, we recommend that if no changes are made in the assumptions about other destruction pathways, 32.5% should be used as the fraction of the oxidizer load converted to nitric acid.

Our most conservative estimate of the source strength would be to use the fuel-to-interface ratio of 1.6:1 and an initial fuel temperature of 400 K. This gives 16% of the initial oxidizer remaining in the cloud, and 4% of the hydrazine remaining, as seen in Table 3. This estimate is probably too conservative, however, since it ignores the possibility of fuel bin ignition, something considered likely by both this study and the L-M report. Our simulations indicate that the fuel nearest the interface will certainly ignite, and that this will, in turn, set off some, but not all, of the remaining fuel. If we make the somewhat arbitrary assumption that half the fuel outside the interface is consumed in this way, we can make a reasonable approximation of the most likely source strength. If we use the 400 K initial fuel bin temperature to model the unignited fuel and the 700 K initial fuel temperature (the lowest temperature at which the fuel bin ignites) to represent the ignited fuel, and then average the two results, we get 24% of the initial oxidizer remaining and 2% of the initial fuel remaining.

These source strength numbers are roughly half those given by L-M for hydrazine and oxidizer, and about one-third those presently used for the oxidizer in REEDM. Hydrazine itself will be destroyed rapidly after the cloud mixes with ambient ozone. UDMH, however, which is present in the actual fuel mix but was ignored here to produce results more quickly, forms toxic products upon reaction with ozone and could be a hazard.

7.2 Future Work

There are several areas that have been neglected in order to rapidly build a model and to get prompt results. These features should be added to the model to increase its credibility and to get a more detailed picture of aborts. The areas are:

- Add HCl chemistry (from the solid rocket boosters).
- Add reactions on aerosol solids.
- Add HCN chemistry to UDMH mechanism.
- Vary the mixing rate to get scaling information for field tests.
- Perform validation experiments. This could include field release experiments or laboratory experiments on the conversion of NO_x to nitric acid.
- More information is needed on the fraction of hydrazine that will burn in an abort.

8. Validation Data

With any model, it is important to verify, as much as possible, that the predictions will be in agreement with the actual behavior of the system. Data on the composition of launch clouds and plumes are scarce. We do, however, have two field situations for which data are available to compare to our model's results. The two cases are for the HCl cloud after a normal launch, and for a cold spill of nitrogen tetroxide.

A measurement of gaseous and total HCl was made after a Shuttle launch in 1981.[16] The field measurements were made on two portions of the exhaust cloud, a high cloud that broke through the inversion layer and a low cloud that stayed at 650–950 m altitude, below the inversion layer. The ambient conditions for the low cloud were a temperature of 290 K and 70 % relative humidity. For the Shuttle launch, we fit the data on total HCl concentration vs. time to get the observed dispersion rate. In Figure 18, the field measurement data on gaseous HCl and the fraction of HCl in the aeresol

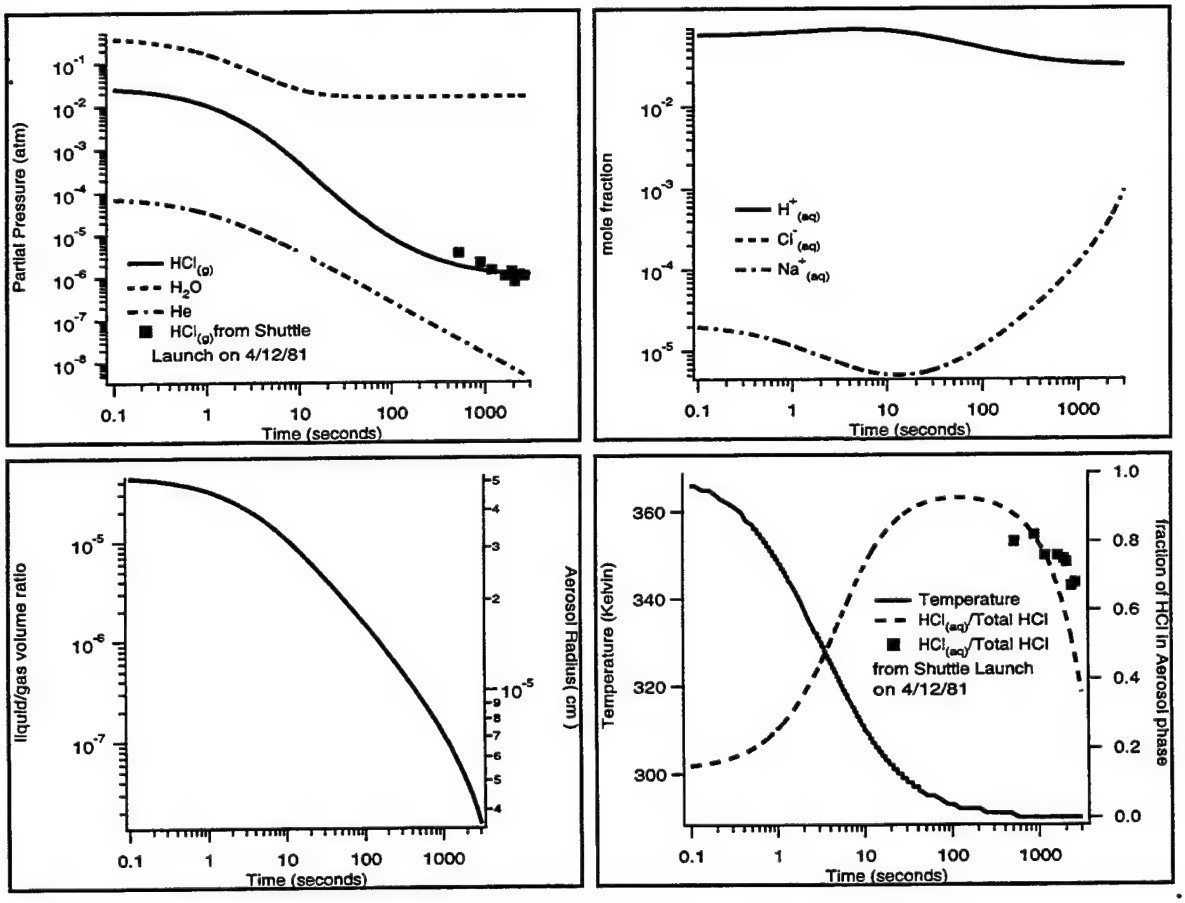

Figure 18. Comparison of model results with field data for a Shuttle HCl launch cloud. Fitting the dispersion rate gives good agreement with the gas/aerosol partitioning.

are plotted (solid squares) against the model predictions. The aerosol fraction was calculated from the difference between the total HCl and gas-phase HCl divided by the total. The agreement between the model predictions and the field measurements is excellent.

For the case of N_2O^4, a series of cold spills were conducted in the desert in the early 1980's (the Eagle Test Series[17,18,19]). In this series of tests, approximately 5000 kg of N_2O_4 was spilled in a single run, and diagnostics downwind monitored the plume size and composition. An array of NO_x detectors 25 m downwind of the spill site were used to estimate the total flux of NO_x at that point.

The mass flux measured by these detectors was only 20% of the mass released at the spill site. The authors of the Eagle report ascribe most of this "missing mass" to conversion to nitric acid, which was seen in abundance at the site but not measured quantitatively. The authors also state that perhaps 50% of the missing NO_x might be attributed to the plume not passing through the array. Thus, from 50% to 80% of the spilled N_2O_4 appears to have converted to HNO_3 by the time the plume reached the array. Since the wind velocity was recorded, we know that this time was from 4.5 to 6.8 s in the tests. Thus, the Eagle Series test suggests that conversion to nitric acid is quite rapid in the field. This is illustrated in Figure 19, which compares the model results with the Eagle data points. Thus, our model is consistent with the observations.

The scarcity of existing field data on launch clouds and the difficulty of obtaining large-scale field data lead us to conclude that laboratory scale experiments are required to provide further validation of this model.

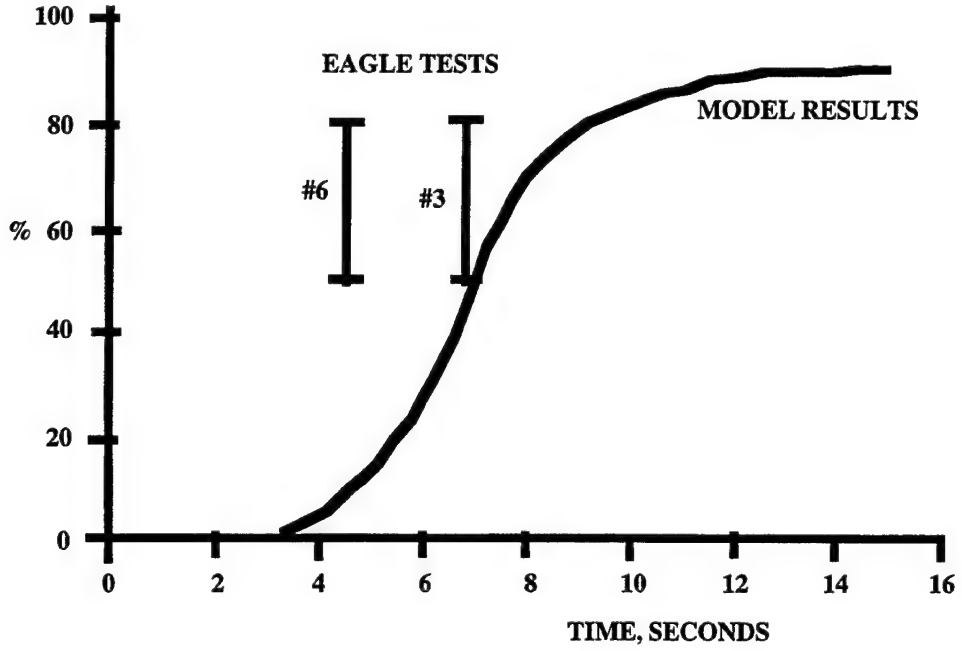

Figure 19. Comparison of model results with field data from the Eagle series N2O4 spills in the desert. The model accounts for the "missing" NO_x.

References

1. S. P. Prince and D. W. Banning, " Launch Vehicle Abort Source Strength Model— Final Report—Source Characterization," MCR-94-506 Martin Marietta Astronautics, Denver, CO, June 28, 1994. (See also R. W. Knight and S. P. Prince, "Atmospheric Dispersion of Solid and Liquid Rocket Propellants," AFESC Report ESL-TR-88-35, January 1989.)

2. E. C. Tuazon, et al., "Atmospheric Reaction Mechanisms of Amine Fuels," Report No. ESL-TR-82-17, U. S. Air Force Engineering and Services Center, Tyndall Air Force Base, Florida, March 1982.

3. B. B. Brady and L. R. Martin, "Use of SURFACE CHEMKIN to Model Multiphase Atmospheric Chemistry: Application to Nitrogen Tetroxide Spills," Atmospheric Environment, 29, 715-26, 1995.

4. J-Y Park and Lee, Y-N, "Solubility and Decomposition Kinetics of Nitrous Acid in Aqueous Solution," *J. Phys. Chem.* **92**, 6294-6302 (1988).

5. *NIST Chemical Kinetics Database Version 4.0* (1992) U. S. Department of Commerce National Institute of Standards and Technology, Standard Reference Data Program, Gaithersburg, MD 20899.

6. C. T. Bowman, R. K. Hanson, D. F. Davidson, W. C. Gardiner, Jr., V. Lissianski, G. P. Smith, D. M. Golden, M. Frenklach, and M. Goldenberg, GRI Mech 2.11, http://www.me.berkeley.edu/gri_mech/.

7. M. W. Chase, Jr., et al., "JANAF Thermochemical Tables Third Edition," *J. Phys. Chem. Ref. Data* **14**, Supplement No. 1 (1985).

8. M. E Coltrin, R. J. Kee, and F. M. Rupley, "SURFACE CHEMKIN (Version 4.0): A Fortran Package for Analyzing Heterogeneous Chemical Kinetics at a Solid-Surface - Gas-Phase Interface," *Sandia Report* SAND90-8003B.UC-401, 91pp (1991).

9. R. J. Kee, F. M. Rupley, and J. A. Miller, "The CHEMKIN Thermodynamic Data Base," *Sandia Report* SAND87-8215B . UC-4, 155 pp (1991a).

10. R. J.,Kee, F. M. Rupley, and J. A. Miller, "CHEMKIN-II: A Fortran Chemical Kinetics Package for the Analysis of Gas-Phase Chemical Kinetics," *Sandia Report* SAND89-8009 . UC-401, 127 pp (1991b).

11. *National Research Council (1928) International Critical Tables of Numerical Data, Physics, Chemistry and Technology Volume III*, E. W. Washburn, Ed. McGraw-Hill, New York 304-305.

12. S. Schwartz, "Gas-Aqueous Reactions of Sulfur and Nitrogen Oxides in Liquid-Water Clouds," in *SO_2, NO and NO_2 Oxidation Mechanisms: Atmospheric Considerations*, J. G. Calvert, Ed. Butterworth Publishers, Boston pp 173 -208 (1984).

13. S. Z. Levine and S. Schwartz, "In-Cloud and Below-Cloud Scavenging of nitric Acid Vapor," *Atmospheric Environment* **16**, 1725-1734 (1982).

14. S. Mertes and A. Wahner, "Uptake of Nitrogen Dioxide and Nitrous Acid on Aqueous Surfaces," *J. Phys. Chem.* **99**, 14000-14006 (1995).

15. J. J. P. Stewart, MOPAC 6.0, United States Air Force Academy, 1990.

16. D. I. Sebacher, R. J. Bendura, and G. L. Gregory, "Hydrogen Chloride Measurements in the Space Shuttle Exhaust Cloud - First Launch, April 12, 1981," *J. Spacecraft* **19**, 366-70 (1982).

17. T. G. McRae, H. C. Goldwire, Jr., and R. P. Koopman, "The Evaporation and Gaseous Dispersion of Large-Scale Releases of Nitrogen Tetroxide, Lawrence Livermore National Laboratory Report UCRL-89687, 22 pp (1984).

18. T. G. McRae, "Analysis and Model/Data Comparisons of Large-Scale Releases of Nitrogen Tetroxide," Lawrence Livermore National Laboratory Report UCID-20388, 78 pp (1985).

19. T. G. McRae, R. T. Cederwall, D. L. Ermak, H. C. Goldwire, Jr., D. L. Hipple, G. W. Johnson, R. P. Koopman, J. W. McClure, and L. K. Morris, "Eagle Series Data Report: 1983 Nitrogen Tetroxide," Lawrence Livermore National Laboratory Report UCID-20063-Rev.1, 141 pp (1987).

Appendix—The Chemical Model—Details

Model Description

The computer model is based on the SURFACE CHEMKIN subroutine package developed by R. J. Kee and coworkers of Sandia, Livermore.[8,9,10] This package contains subroutines for calculating thermodynamic properties, equilibrium constants, rates, and unit conversions, for parsing character data such as species and element names, and reaction mechanisms. The subroutine LSODE (Livermore Solver of Ordinary Differential Equations) is used for solving the set of differential equations. SURFACE CHEMKIN is a set of software tools and a subroutine library designed to help create a program to solve a specific chemical kinetics or thermodynamics problem. The package is designed to help solve a group of differential equations subject to a set of constraints; various properties of the system may be extracted along the way. One needs to write the program that describes the chemical system of interest and calls the appropriate subroutines to do the calculations. Multiple surface and bulk phases can be included. Surface rates are scaled by the ratio of surface area to gas-phase volume. The package is designed to model chemical vapor deposition. We wrote a driver program incorporating some changes in the calculation method, added some new subroutines, and modified some of the original routines. The resulting program is well adapted to atmospheric chemistry. Our alterations are described in more detail below.

The plume model is adiabatic with respect to the plume. The atmosphere is treated as a large bath and is isothermal. CHEMKIN calculates the enthalpy of each species in the model. As species are created or destroyed through reaction, they add or subtract energy from the plume; mixing with the air also effects the energy balance. When species leave the plume or enter from the atmosphere, they also carry energy, which is tracked. This net change in energy is divided by the heat capacity of the plume to obtain the temperature change for each integration step. This energy conservation equation is included as a governing equation, or constraint, for SURFACE CHEMKIN.

The governing equation for temperature, alluded to above, is based on conservation of energy, and is included here for reference.

$$\frac{\partial T}{\partial t} = \frac{\sum_{i=1}^{N} H_i^m m_i \left[\frac{\partial n_i^g}{\partial t} + \frac{\partial n_i^s}{\partial t} A_R + \frac{\partial n_i^\ell}{\partial t} V_R \right] + \left(T^{Air} - T \right) \frac{\partial \sigma_p}{\sigma_p \partial t} C_p^{Air}}{\left(C_p^g \rho + C_p^\ell m_\ell \right)}$$

The preceding equation describes the change in the plume temperature with time. The numerator in this equation is the total enthalpy change for the plume in time interval ∂t. The summation is over species i, where N is the total number of species considered. H_i^m is the enthalpy in mass units, m_i is the molecular weight of species i, and n_i^{phase} is the number of moles produced by gas, g, surface, s,

or liquid phase, ℓ, reactions per unit volume (area for phase = s); the product $H_i^m m_i \frac{\partial n_i^g}{\partial t}$ represents the heat gained or lost to the plume due to the production (or consumption) of a particular chemical species in gas-phase reactions in the time interval ∂t. The rate of species production from surface reactions, $\frac{\partial n_i^s}{\partial t}$, is normalized by A_R, the ratio of surface area to gas-phase volume. V_R is the ratio of liquid-phase volume to gas-phase volume, which normalizes the rate of species production from bulk-phase reactions, $\frac{\partial n_i^\ell}{\partial t}$. T is the temperature, σ_p is the cross-sectional area of the plume, and C_p is heat capacity. The term $\left(T^{Air} - T\right)\frac{\partial \sigma_p}{\sigma_p \partial t} C_p^{Air}$ represents the heat required to bring ambient air, which is mixing into the plume, to the same temperature as the plume gases. The superscript *Air* refers to quantities in the undisturbed air outside the plume. The denominator in the above equation represents the specific heat of the plume and is made up of the specific heat of the gas phase, $C_p^g \rho$, and condensed phase, $C_p^\ell m_\ell$, portions, where ρ is the gas-phase density, and the total mass in the liquid phase per unit volume of gas is m_ℓ The heat capacity of the surface "phase" is negligible and is ignored.

The remaining constraints are based on conservation of mass and are broken down into separate equations for each species in each phase. The governing equation for gas-phase species is

$$\frac{\partial Y_i}{\partial t} = \frac{m_i}{\rho}\left[\frac{\partial n_i^g}{\partial t} + \frac{\partial n_i^s}{\partial t} A_R + \frac{\partial n_i^\ell}{\partial t} V_R\right] + \left(Y_i^{Air} - Y_i^g\right)\frac{\partial \sigma_p}{\sigma_p \partial t} \quad .$$

The symbol Y is used for the gas-phase mass fraction. The first term in this equation is the molar changes due to reaction converted to a mass fraction, and the second term is the effect of dilution on plume species. This equation has a similar structure to the numerator of the first governing equation.

The equation for surface species in terms of site fraction, X_i, is similar. There is also a correction for coverage, where the density of surface sites in a given surface phase j is given by Γ_j, and the number of sites occupied by a given species is σ_i. Large molecules could occupy several sites, but all the species in this model are small molecules with $\sigma_i = 1$. Only one surface phase is used in our model. There is an equation like the following one for each surface species.

$$\frac{\partial X_i}{\partial t} = \left(\frac{\partial n_i^s}{\partial t} + \frac{\partial n_i^\ell}{\partial t} V_R\right)\frac{\sigma_i}{\Gamma_j}$$

The equations for liquid species are also similar, but given in mass, z_i. A term for dry deposition is added. Multiple bulk phases are possible, but only one is used here. An equation like the following is generated for each species in the liquid phase.

$$\frac{\partial z_i}{\partial t} = m_i\left[\frac{\partial n_i^s}{\partial t}A_R + \frac{\partial n_i^\ell}{\partial t}V_R\right] + \left(z_i^{Air} - z_i^\ell\right)\frac{\partial \sigma_p}{\sigma_p \partial t} - z_i^\ell\left[-v_d t \Big/ (h_0 + h't)\right]$$

This complete set of constraints is used in solving the differential equations from the kinetics for each time step in the simulation.

We have made several changes to the Sandia package. To model an aerosol, we keep track of the total condensed volume and let the surface area vary with the volume and droplet size. We created a separate set of pure bulk-phase (non-surface) reactions whose rates are scaled by the ratio of condensed phase volume to gas volume.

We also needed to add the effect of atmospheric dispersion. We use a simple Gaussian plume model; the centerline concentration is given by

$$C^0 = \frac{R}{v}\left(\frac{1}{\pi\sigma_y\sigma_z}\right),$$

where C_i^0 is the initial centerline concentration of propellant, and σ_y and σ_z are the plume spreading parameters for the horizontal and vertical directions. For simplicity, the spreading parameters, σ_y and σ_z, are taken to increase linearly with time: $\sigma_z = \sigma_{z(0)} + ax; \sigma_y = \sigma_{y(0)} + bx$; for this case, $\sigma_z = 1 + 0.07x$(meters) and σ_y(meters), which corresponds roughly to the Pasquill stability class "C," a typical condition at Vandenburg. This essentially means that in the absence of reactions, the concentration drops with the square of time. The time derivative of this equation is included in the model, and is represented by the term $\frac{\partial \sigma_p}{\sigma_p \partial t}$ in several of the governing equations.

Complete List of Reactions

The complete gas-phase reaction set now includes 298 gas-phase reactions and 13 heterogeneous reactions, shown in the Tables 1A and 2A.

Table 1A: Surface and Bulk Reactions

Surface Reactions	k (mole^{-1} s^{-1}) or γ
$H_2O + H_2O(A) \leftrightarrow H_2O(A) + H_2O(L)$	1.0
$H_2O + NaCl(A) \leftrightarrow H_2O(A) + NaCl(S)$	1.0
$N_2O_5 + H_2O(A) \leftrightarrow HNO_3(A) + HNO_3(L)$	1.0
$N_2O_4 + H_2O(A) \leftrightarrow HNO_3(L) + HONO(A)$	1.0
$NO_2 + H_2O(A) \leftrightarrow NO_2(L) + H_2O(A)$	1.0
$NO + H_2O(A) \leftrightarrow NO(L) + H_2O(A)$	1.0
$HNO_3 + H_2O(A) \leftrightarrow HNO_3(A) + H_2O(L)$	1.0
$HONO + H_2O(A) \leftrightarrow HONO(A) + H_2O(L)$	1.0
$HNO_3(A) + H_2O(L) \leftrightarrow H_2O(A) + HNO_3(L)$	1.0e10
$HONO(A) + H_2O(L) \leftrightarrow H_2O(A) + HONO(L)$	1.0e10
$NaCl(A) + H_2O(L) \leftrightarrow NaCl(S) + H_2O(A)$	1.0e10
Bulk Reactions	
$2NO_2(L) + H_2O(L) \leftrightarrow HNO_3(L) + HONO(L)$	8.4e10
$2HONO(L) \leftrightarrow NO_2(L) + NO(L) + H_2O(L)$	1.3e4

The liquid-phase rates are in cm^{3}mole^{-1} sec^{-1} and must be multiplied by $(0.0555)^2$ to be used correctly for the bulk phase by the program. Liquid-phase rates are from Park and Lee (Ref. 4). The gas-surface reactions and the surface-bulk reactions are taken not to be rate limiting except for the N_2O_4 + water reaction, as described in the text.

Table 2A: Gas Phase Reactions

Reactions Considered			A	b	E
			(k = A T**b exp(-E/RT))		
1. H2+O2=2OH			1.70E+13	.0	47780.0
2. H2O2+M=OH+OH+M			1.30E+17	.0	45500.0
3. O3+NO2=NO3+O2			1.14E+11	.0	5052.0
4. O+NO2=O2+NO			3.98E+12	.0	-178.0
5. O+NO2+M=NO3+M			5.32E+15	.0	-1057.0
6. O+O2+M=O3+M			3.35E+13	.0	-972.0
7. OH+NO2+M=HNO3+M			3.04E+16	.0	-1824.0
8. N2O5=NO2+NO3			1.59E+15	.0	22300.0
9. N2O4+M=2NO2+M			1.46E+17	.0	10560.0
N2O4	Enhanced by	1.000E+01			
N2H4	Enhanced by	1.000E+01			
10. 2HONO=NO2+NO+H2O			1.00E+13	.0	8528.0
11. NO2+HV=>NO+O			9.00E-03	.0	.0
12. NO3+HV=>NO2+O			1.80E-01	.0	.0
13. O3+HV=>O+O2			3.60E-04	.0	.0
14. O3+HV=>O1D+O2			1.60E-05	.0	.0
15. O1D+M=O+M			1.74E+13	.0	.0
16. O1D+H2O=2OH			1.32E+14	.0	.0

16. O1D+H2O=2OH			1.32E+14	.0	.0
17. OH+NO2=HNO3			9.62E+12	.0	.0
18. 2NO+O2=2NO2			1.45E+10	.0	.0
19. NO+NO=N2+O2			1.78E+11	.5	60520.0
20. NO+NO=N2O+O			9.04E+12	.0	65552.0
21. NO+HO2=NO2+OH			2.11E+12	.0	-479.0
22. NO+NO3=2NO2			6.32E+12	.0	-443.0
23. NO+O3=NO2+O2			1.47E+12	.0	2874.0
24. NO+H2O2=HONO+OH			1.00E+14	.0	.0
25. NO2+NO3+M=N2O5+M			2.86E+16	.0	-2111.0
26. NO2+H=NO+OH			3.50E+14	.0	1500.0
27. N2O+O=N2+O2			4.50E+13	.0	24101.0
28. N2O+H=OH+N2			7.59E+13	.0	15103.0
29. N2O+M=N2+O			1.62E+14	.0	51600.0
30. N2O+OH=N2+HO2			2.00E+12	.0	10000.0
31. O+N2=NO+N			3.11E+10	1.0	74600.0
32. N+O2=NO+O			5.12E+09	1.0	6140.0
33. N+OH=NO+H			2.34E+13	.0	-170.0
34. HNO+M=H+NO+M			1.50E+16	.0	48680.0
H2O	Enhanced by	1.000E+01			
H2	Enhanced by	2.000E+00			
O2	Enhanced by	2.000E+00			
N2	Enhanced by	2.000E+00			
35. HNO+OH=NO+H2O			3.60E+13	.0	.0
36. HNO+H=H2+NO			5.00E+12	.0	.0
37. HNO+NH2=NH3+NO			2.00E+13	.0	1000.0
38. HNO+HNO=N2O+H2O			3.95E+12	.0	5000.0
39. HNO+NO=N2O+OH			2.00E+12	.0	26000.0
40. N2H4=NH2+NH2			3.98E+13	.0	53001.0
41. N2H4+OH=H2O+N2H3			2.65E+13	.0	-230.0
42. N2H4+NH2=NH3+N2H3			4.68E+12	.0	2144.0
43. N2H4+NO2=N2H3+HONO			1.50E+05	.0	.0
44. N2H4+NO=N2H3+HNO			1.50E+03	.0	.0
45. N2H3+NO2=N2H2+HONO			1.00E+14	.0	.0
46. N2H3+NO=N2H2+HNO			1.00E+14	.0	.0
47. N2H3+H=NH2+NH2			1.60E+12	.0	.0
48. N2H3+N2H3=NH3+NH3+N2			1.00E+13	.0	.0
49. N2H2+NO2=NNH+HONO			1.00E+14	.0	.0
50. N2H2+NO=NNH+HNO			1.00E+14	.0	.0
51. N2H2+M=NNH+H+M			5.00E+16	.0	50000.0
H2O	Enhanced by	1.500E+01			
H2	Enhanced by	2.000E+00			
O2	Enhanced by	2.000E+00			
N2	Enhanced by	2.000E+00			
52. N2H2+H=NNH+H2			5.00E+13	.0	1000.0
53. N2H2+O=NH2+NO			1.00E+13	.0	.0
54. N2H2+O=NNH+OH			2.00E+13	.0	1000.0
55. N2H2+OH=NNH+H2O			1.00E+13	.0	1000.0
56. N2H2+NO=NH2+N2O			3.00E+12	.0	.0
57. N2H2+NH=NNH+NH2			1.00E+13	.0	1000.0
58. N2H2+NH2=NNH+NH3			1.00E+13	.0	1000.0

59. NNH=N2+H	1.00E+04	.0	.0
60. NNH+NO=N2+HNO	5.00E+13	.0	.0
61. NNH+H=N2+H2	1.00E+14	.0	.0
62. NNH+OH=N2+H2O	5.00E+13	.0	.0
63. NNH+NH2=N2+NH3	5.00E+13	.0	.0
64. NNH+NH=N2+NH2	5.00E+13	.0	.0
65. NNH+O=N2O+H	1.00E+14	.0	.0
66. NH3+OH=NH2+H2O	2.04E+06	2.0	566.0
67. NH2+H2=NH3+H	5.33E+13	.0	9503.0
68. NH2+O=H2+NO	5.00E+12	.0	.0
69. NH2+O=NH+OH	7.00E+12	.0	.0
70. NH2+O=HNO+H	4.50E+13	.0	.0
71. NH2+O2=NH+HO2	1.00E+14	.0	50000.0
72. NH2+O2=HNO+OH	4.73E+14	.0	36100.0
73. NH2+OH=H2O+NH	9.01E+07	1.5	-457.0
74. NH2+OH=O+NH3	4.06E-04	2.6	-1729.0
75. NH2+H=H2+NH	1.91E+13	.0	.0
76. NH2+H+M=NH3+M	2.20E+18	.0	.0
77. NH2+N=H+H+N2	7.00E+13	.0	.0
78. NH2+NO=N2+H2O	2.71E+14	-1.2	-1771.0
79. NH2+NO=NNH+OH	1.42E+19	-2.5	1864.0
80. NH2+NH=N2H2+H	1.50E+15	-.5	.0
81. NH2+NH=N2H3	7.00E+13	.0	.0
82. NH2+NH2=N2H2+H2	5.00E+11	.0	.0
83. NH+NH=N2+2H	2.54E+13	.0	.0
84. NH=N+H	2.65E+14	.0	75500.0
85. NH+O=OH+N	7.00E+12	.0	.0
86. NH+O=NO+H	7.00E+13	.0	.0
87. NH+O2=NO+OH	4.50E+13	.0	9940.0
88. NH+O2=O+HNO	1.00E+13	.0	1000.0
89. NH+OH=H2O+N	2.00E+09	1.2	6.0
90. NH+OH=H+HNO	2.00E+13	.0	.0
91. NH+H=H2+N	3.01E+13	.0	.0
92. NH+N=N2+H	3.00E+13	.0	.0
93. NH+NH=N2H2	1.00E+14	.0	.0
94. NH+NH3+M=N2H4+M	1.00E+12	.0	.0
95. NH+NO=N2+OH	2.00E+13	.0	.0
96. NH+NO=H+N2O	8.00E+13	.0	29400.0
97. (CH3)2N2H2+O3=(CH3)2N2H+OH+O2	8.40E+08	.0	.0
98. (CH3)2N2H+O3=(CH3)2N2HO+O2	6.00E+09	.0	.0
99. (CH3)2N2HO+O2=(CH3)2N2O+HO2	6.00E+09	.0	.0
100. (CH3)2N2H2+OH=(CH3)2N2H+H2O	3.00E+13	.0	.0
101. (CH3)2N2O+hv=>(CH3)2N+NO	3.33E-03	.0	.0
102. (CH3)2N2H2+NO2=HONO+(CH3)2N2H	1.38E+07	.0	.0
103. (CH3)2N2H+NO2=(CH3)2N2+HONO	6.00E+09	.0	.0
104. 2(CH3)2N2=(CH3)2N4(CH3)2	6.00E+10	.0	.0
105. (CH3)2N2O+OH=(CH3)2N+HONO	1.80E+12	.0	.0
106. (CH3)2N2O+M=(CH3)2N+NO+M	6.25E+15	.0	49995.0
107. (CH3)2N+O2=CH3NCH2+HO2	6.00E+07	.0	.0
108. CH3NCH2+O3=CH3NO2+CH2O	6.00E+09	.0	.0
109. CH3NO2+hv=CH3O+NO	1.00E-03	.0	.0

110. CH3NO2+M=CH2O+HNO+M			1.00E+10	.0	31800.0
111. CH3NO2+M=CH3O+NO+M			6.30E+15	.0	41220.0
112. CH3NO2+M=CH3+NO2+M			1.78E+16	.0	58499.0
113. (CH3)2N2H2+OH=(CH3)(CH2)N2H2+H2O			2.40E+13	.0	.0
114. (CH3)(CH2)N2H2=CH3NCH2+NH2			3.98E+17	.0	9931.0
115. (CH3)2N2H2=(CH3)2N+NH2			3.98E+17	.0	62988.0
116. (CH3)2N2H=NH+(CH3)2N			3.98E+17	.0	62996.0
117. (CH3)2N+OH=CH3NCH2+H2O			6.00E+12	.0	.0
118. CH3+(CH3)2N=CH3NCH2+CH4			7.90E+12	.0	.0
119. CH3+(CH3)2N=(CH3)3N			1.75E+13	.0	.0
120. (CH3)2N2H2+H=(CH3)2N2H+H2			2.00E+12	.0	2200.0
121. (CH3)2N2H2+H=(CH3)(CH2)N2H2+H2			1.00E+13	.0	5300.0
122. 2O+M<=>O2+M			1.20E+17	-1.0	.0
H2	Enhanced by	2.400E+00			
H2O	Enhanced by	1.540E+01			
CH4	Enhanced by	2.000E+00			
CO	Enhanced by	1.750E+00			
CO2	Enhanced by	3.600E+00			
C2H6	Enhanced by	3.000E+00			
Ar	Enhanced by	8.300E-01			
123. O+H+M<=>OH+M			5.00E+17	-1.0	.0
H2	Enhanced by	2.000E+00			
H2O	Enhanced by	6.000E+00			
CH4	Enhanced by	2.000E+00			
CO	Enhanced by	1.500E+00			
CO2	Enhanced by	2.000E+00			
C2H6	Enhanced by	3.000E+00			
Ar	Enhanced by	7.000E-01			
124. O+H2<=>H+OH			5.00E+04	2.7	6290.0
125. O+HO2<=>OH+O2			2.00E+13	.0	.0
126. O+H2O2<=>OH+HO2			9.63E+06	2.0	4000.0
127. O+CH<=>H+CO			5.70E+13	.0	.0
128. O+CH2<=>H+HCO			8.00E+13	.0	.0
129. O+CH2(S)<=>H2+CO			1.50E+13	.0	.0
130. O+CH2(S)<=>H+HCO			1.50E+13	.0	.0
131. O+CH3<=>H+CH2O			8.43E+13	.0	.0
132. O+CH4<=>OH+CH3			1.02E+09	1.5	8600.0
133. O+CO+M<=>CO2+M			6.02E+14	.0	3000.0
H2	Enhanced by	2.000E+00			
O2	Enhanced by	6.000E+00			
H2O	Enhanced by	6.000E+00			
CH4	Enhanced by	2.000E+00			
CO	Enhanced by	1.500E+00			
CO2	Enhanced by	3.500E+00			
C2H6	Enhanced by	3.000E+00			
Ar	Enhanced by	5.000E-01			
134. O+HCO<=>OH+CO			3.00E+13	.0	.0
135. O+HCO<=>H+CO2			3.00E+13	.0	.0
136. O+CH2O<=>OH+HCO			3.90E+13	.0	3540.0
137. O+CH2OH<=>OH+CH2O			1.00E+13	.0	.0
138. O+CH3O<=>OH+CH2O			1.00E+13	.0	.0

139. O+CH3OH<=>OH+CH2OH			3.88E+05	2.5	3100.0
140. O+CH3OH<=>OH+CH3O			1.30E+05	2.5	5000.0
141. O+C2H<=>CH+CO			5.00E+13	.0	.0
142. O+C2H2<=>H+HCCO			1.02E+07	2.0	1900.0
143. O+C2H2<=>OH+C2H			4.60E+19	-1.4	28950.0
144. O+C2H2<=>CO+CH2			1.02E+07	2.0	1900.0
145. O+C2H3<=>H+CH2CO			3.00E+13	.0	.0
146. O+C2H4<=>CH3+HCO			1.92E+07	1.8	220.0
147. O+C2H5<=>CH3+CH2O			1.32E+14	.0	.0
148. O+C2H6<=>OH+C2H5			8.98E+07	1.9	5690.0
149. O+HCCO<=>H+2CO			1.00E+14	.0	.0
150. O+CH2CO<=>OH+HCCO			1.00E+13	.0	8000.0
151. O+CH2CO<=>CH2+CO2			1.75E+12	.0	1350.0
152. O2+CO<=>O+CO2			2.50E+12	.0	47800.0
153. O2+CH2O<=>HO2+HCO			1.00E+14	.0	40000.0
154. H+O2+M<=>HO2+M			2.80E+18	-.9	.0
O2	Enhanced by	0.000E-01			
H2O	Enhanced by	0.000E-01			
CO	Enhanced by	7.500E-01			
CO2	Enhanced by	1.500E+00			
C2H6	Enhanced by	1.500E+00			
N2	Enhanced by	0.000E-01			
Ar	Enhanced by	0.000E-01			
155. H+2O2<=>HO2+O2			3.00E+20	-1.7	.0
156. H+O2+H2O<=>HO2+H2O			9.38E+18	-.8	.0
157. H+O2+N2<=>HO2+N2			3.75E+20	-1.7	.0
158. H+O2+Ar<=>HO2+Ar			7.00E+17	-.8	.0
159. H+O2<=>O+OH			8.30E+13	.0	14413.0
160. 2H+M<=>H2+M			1.00E+18	-1.0	.0
H2	Enhanced by	0.000E-01			
H2O	Enhanced by	0.000E-01			
CH4	Enhanced by	2.000E+00			
CO2	Enhanced by	0.000E-01			
C2H6	Enhanced by	3.000E+00			
Ar	Enhanced by	6.300E-01			
161. 2H+H2<=>2H2			9.00E+16	-.6	.0
162. 2H+H2O<=>H2+H2O			6.00E+19	-1.3	.0
163. 2H+CO2<=>H2+CO2			5.50E+20	-2.0	.0
164. H+OH+M<=>H2O+M			2.20E+22	-2.0	.0
H2	Enhanced by	7.300E-01			
H2O	Enhanced by	3.650E+00			
CH4	Enhanced by	2.000E+00			
C2H6	Enhanced by	3.000E+00			
Ar	Enhanced by	3.800E-01			
165. H+HO2<=>O+H2O			3.97E+12	.0	671.0
166. H+HO2<=>O2+H2			2.80E+13	.0	1068.0
167. H+HO2<=>2OH			1.34E+14	.0	635.0
168. H+H2O2<=>HO2+H2			1.21E+07	2.0	5200.0
169. H+H2O2<=>OH+H2O			1.00E+13	.0	3600.0
170. H+CH<=>C+H2			1.10E+14	.0	.0
171. H+CH2(+M)<=>CH3(+M)			2.50E+16	-.8	.0

Low pressure limit: 0.32000E+28 -0.31400E+01 0.12300E+04
TROE centering: 0.68000E+00 0.78000E+02 0.19950E+04 0.55900E+04
H2 Enhanced by 2.000E+00
H2O Enhanced by 6.000E+00
CH4 Enhanced by 2.000E+00
CO Enhanced by 1.500E+00
CO2 Enhanced by 2.000E+00
C2H6 Enhanced by 3.000E+00
Ar Enhanced by 7.000E-01

172. H+CH2(S)<=>CH+H2 3.00E+13 .0 .0
173. H+CH3(+M)<=>CH4(+M) 1.27E+16 -.6 383.0
Low pressure limit: 0.24770E+34 -0.47600E+01 0.24400E+04
TROE centering: 0.78300E+00 0.74000E+02 0.29410E+04 0.69640E+04
H2 Enhanced by 2.000E+00
H2O Enhanced by 6.000E+00
CH4 Enhanced by 2.000E+00
CO Enhanced by 1.500E+00
CO2 Enhanced by 2.000E+00
C2H6 Enhanced by 3.000E+00
Ar Enhanced by 7.000E-01
174. H+CH4<=>CH3+H2 6.60E+08 1.6 10840.0
175. H+HCO(+M)<=>CH2O(+M) 1.09E+12 .5 -260.0
Low pressure limit: 0.13500E+25 -0.25700E+01 0.14250E+04
TROE centering: 0.78240E+00 0.27100E+03 0.27550E+04 0.65700E+04
H2 Enhanced by 2.000E+00
H2O Enhanced by 6.000E+00
CH4 Enhanced by 2.000E+00
CO Enhanced by 1.500E+00
CO2 Enhanced by 2.000E+00
C2H6 Enhanced by 3.000E+00
Ar Enhanced by 7.000E-01
176. H+HCO<=>H2+CO 7.34E+13 .0 .0
177. H+CH2O(+M)<=>CH2OH(+M) 5.40E+11 .5 3600.0
Low pressure limit: 0.12700E+33 -0.48200E+01 0.65300E+04
TROE centering: 0.71870E+00 0.10300E+03 0.12910E+04 0.41600E+04
H2 Enhanced by 2.000E+00
H2O Enhanced by 6.000E+00
CH4 Enhanced by 2.000E+00
CO Enhanced by 1.500E+00
CO2 Enhanced by 2.000E+00
C2H6 Enhanced by 3.000E+00
178. H+CH2O(+M)<=>CH3O(+M) 5.40E+11 .5 2600.0
Low pressure limit: 0.22000E+31 -0.48000E+01 0.55600E+04
TROE centering: 0.75800E+00 0.94000E+02 0.15550E+04 0.42000E+04
H2 Enhanced by 2.000E+00
H2O Enhanced by 6.000E+00
CH4 Enhanced by 2.000E+00
CO Enhanced by 1.500E+00
CO2 Enhanced by 2.000E+00
C2H6 Enhanced by 3.000E+00
179. H+CH2O<=>HCO+H2 2.30E+10 1.1 3275.0

```
180. H+CH2OH(+M)<=>CH3OH(+M)                    1.80E+13   .0       .0
   Low pressure limit:  0.30000E+32 -0.48000E+01  0.33000E+04
   TROE centering:      0.76790E+00  0.33800E+03  0.18120E+04  0.50810E+04
     H2              Enhanced by    2.000E+00
     H2O             Enhanced by    6.000E+00
     CH4             Enhanced by    2.000E+00
     CO              Enhanced by    1.500E+00
     CO2             Enhanced by    2.000E+00
     C2H6            Enhanced by    3.000E+00
181. H+CH2OH<=>H2+CH2O                          2.00E+13   .0       .0
182. H+CH2OH<=>OH+CH3                           1.20E+13   .0       .0
183. H+CH2OH<=>CH2(S)+H2O                       6.00E+12   .0       .0
184. H+CH3O(+M)<=>CH3OH(+M)                     5.00E+13   .0       .0
   Low pressure limit:  0.86000E+29 -0.40000E+01  0.30250E+04
   TROE centering:      0.89020E+00  0.14400E+03  0.28380E+04  0.45569E+05
     H2              Enhanced by    2.000E+00
     H2O             Enhanced by    6.000E+00
     CH4             Enhanced by    2.000E+00
     CO              Enhanced by    1.500E+00
     CO2             Enhanced by    2.000E+00
     C2H6            Enhanced by    3.000E+00
185. H+CH3O<=>H+CH2OH                           3.40E+06   1.6      .0
186. H+CH3O<=>H2+CH2O                           2.00E+13   .0       .0
187. H+CH3O<=>OH+CH3                            3.20E+13   .0       .0
188. H+CH3O<=>CH2(S)+H2O                        1.60E+13   .0       .0
189. H+CH3OH<=>CH2OH+H2                         1.70E+07   2.1      4870.0
190. H+CH3OH<=>CH3O+H2                          4.20E+06   2.1      4870.0
191. H+C2H(+M)<=>C2H2(+M)                       1.00E+17  -1.0      .0
   Low pressure limit:  0.37500E+34 -0.48000E+01  0.19000E+04
   TROE centering:      0.64640E+00  0.13200E+03  0.13150E+04  0.55660E+04
     H2              Enhanced by    2.000E+00
     H2O             Enhanced by    6.000E+00
     CH4             Enhanced by    2.000E+00
     CO              Enhanced by    1.500E+00
     CO2             Enhanced by    2.000E+00
     C2H6            Enhanced by    3.000E+00
     Ar              Enhanced by    7.000E-01
192. H+C2H2(+M)<=>C2H3(+M)                      5.60E+12   .0       2400.0
   Low pressure limit:  0.38000E+41 -0.72700E+01  0.72200E+04
   TROE centering:      0.75070E+00  0.98500E+02  0.13020E+04  0.41670E+04
     H2              Enhanced by    2.000E+00
     H2O             Enhanced by    6.000E+00
     CH4             Enhanced by    2.000E+00
     CO              Enhanced by    1.500E+00
     CO2             Enhanced by    2.000E+00
     C2H6            Enhanced by    3.000E+00
     Ar              Enhanced by    7.000E-01
193. H+C2H3(+M)<=>C2H4(+M)                      6.08E+12   .3       280.0
   Low pressure limit:  0.14000E+31 -0.38600E+01  0.33200E+04
   TROE centering:      0.78200E+00  0.20750E+03  0.26630E+04  0.60950E+04
     H2              Enhanced by    2.000E+00
```

```
     H2O             Enhanced by   6.000E+00
     CH4             Enhanced by   2.000E+00
     CO              Enhanced by   1.500E+00
     CO2             Enhanced by   2.000E+00
     C2H6            Enhanced by   3.000E+00
     Ar              Enhanced by   7.000E-01
194. H+C2H3<=>H2+C2H2                                 3.00E+13   .0      .0
195. H+C2H4(+M)<=>C2H5(+M)                            1.08E+12   .5   1820.0
   Low pressure limit: 0.12000E+43 -0.76200E+01 0.69700E+04
   TROE centering:     0.97530E+00 0.21000E+03 0.98400E+03 0.43740E+04
     H2              Enhanced by   2.000E+00
     H2O             Enhanced by   6.000E+00
     CH4             Enhanced by   2.000E+00
     CO              Enhanced by   1.500E+00
     CO2             Enhanced by   2.000E+00
     C2H6            Enhanced by   3.000E+00
     Ar              Enhanced by   7.000E-01
196. H+C2H4<=>C2H3+H2                                 1.32E+06   2.5  12240.0
197. H+C2H5(+M)<=>C2H6(+M)                            5.21E+17  -1.0   1580.0
   Low pressure limit: 0.19900E+42 -0.70800E+01 0.66850E+04
   TROE centering:     0.84220E+00 0.12500E+03 0.22190E+04 0.68820E+04
     H2              Enhanced by   2.000E+00
     H2O             Enhanced by   6.000E+00
     CH4             Enhanced by   2.000E+00
     CO              Enhanced by   1.500E+00
     CO2             Enhanced by   2.000E+00
     C2H6            Enhanced by   3.000E+00
     Ar              Enhanced by   7.000E-01
198. H+C2H5<=>H2+C2H4                                 2.00E+12   .0      .0
199. H+C2H6<=>C2H5+H2                                 1.15E+08   1.9  7530.0
200. H+HCCO<=>CH2(S)+CO                               1.00E+14   .0      .0
201. H+CH2CO<=>HCCO+H2                                5.00E+13   .0   8000.0
202. H+CH2CO<=>CH3+CO                                 1.13E+13   .0   3428.0
203. H+HCCOH<=>H+CH2CO                                1.00E+13   .0      .0
204. H2+CO(+M)<=>CH2O(+M)                             4.30E+07   1.5  79600.0
   Low pressure limit: 0.50700E+28 -0.34200E+01 0.84350E+05
   TROE centering:     0.93200E+00 0.19700E+03 0.15400E+04 0.10300E+05
     H2              Enhanced by   2.000E+00
     H2O             Enhanced by   6.000E+00
     CH4             Enhanced by   2.000E+00
     CO              Enhanced by   1.500E+00
     CO2             Enhanced by   2.000E+00
     C2H6            Enhanced by   3.000E+00
     Ar              Enhanced by   7.000E-01
205. OH+H2<=>H+H2O                                    2.16E+08   1.5   3430.0
206. 2OH(+M)<=>H2O2(+M)                               7.40E+13   -.4      .0
   Low pressure limit: 0.23000E+19 -0.90000E+00 -0.17000E+04
   TROE centering:     0.73460E+00 0.94000E+02 0.17560E+04 0.51820E+04
     H2              Enhanced by   2.000E+00
     H2O             Enhanced by   6.000E+00
     CH4             Enhanced by   2.000E+00
```

CO	Enhanced by	1.500E+00			
CO2	Enhanced by	2.000E+00			
C2H6	Enhanced by	3.000E+00			
Ar	Enhanced by	7.000E-01			
207. 2OH<=>O+H2O			3.57E+04	2.4	-2110.0
208. OH+HO2<=>O2+H2O			2.90E+13	.0	-500.0
209. OH+H2O2<=>HO2+H2O			1.75E+12	.0	320.0
Declared duplicate reaction...					
210. OH+H2O2<=>HO2+H2O			5.80E+14	.0	9560.0
Declared duplicate reaction...					
211. OH+C<=>H+CO			5.00E+13	.0	.0
212. OH+CH<=>H+HCO			3.00E+13	.0	.0
213. OH+CH2<=>H+CH2O			2.00E+13	.0	.0
214. OH+CH2<=>CH+H2O			1.13E+07	2.0	3000.0
215. OH+CH2(S)<=>H+CH2O			3.00E+13	.0	.0
216. OH+CH3(+M)<=>CH3OH(+M)			6.30E+13	.0	.0
Low pressure limit:	0.27000E+39	-0.63000E+01	0.31000E+04		
TROE centering:	0.21050E+00	0.83500E+02	0.53980E+04	0.83700E+04	
H2	Enhanced by	2.000E+00			
H2O	Enhanced by	6.000E+00			
CH4	Enhanced by	2.000E+00			
CO	Enhanced by	1.500E+00			
CO2	Enhanced by	2.000E+00			
C2H6	Enhanced by	3.000E+00			
217. OH+CH3<=>CH2+H2O			5.60E+07	1.6	5420.0
218. OH+CH3<=>CH2(S)+H2O			2.50E+13	.0	.0
219. OH+CH4<=>CH3+H2O			1.00E+08	1.6	3120.0
220. OH+CO<=>H+CO2			4.76E+07	1.2	70.0
221. OH+HCO<=>H2O+CO			5.00E+13	.0	.0
222. OH+CH2O<=>HCO+H2O			3.43E+09	1.2	-447.0
223. OH+CH2OH<=>H2O+CH2O			5.00E+12	.0	.0
224. OH+CH3O<=>H2O+CH2O			5.00E+12	.0	.0
225. OH+CH3OH<=>CH2OH+H2O			1.44E+06	2.0	-840.0
226. OH+CH3OH<=>CH3O+H2O			6.30E+06	2.0	1500.0
227. OH+C2H<=>H+HCCO			2.00E+13	.0	.0
228. OH+C2H2<=>H+CH2CO			2.18E-04	4.5	-1000.0
229. OH+C2H2<=>H+HCCOH			5.04E+05	2.3	13500.0
230. OH+C2H2<=>C2H+H2O			3.37E+07	2.0	14000.0
231. OH+C2H2<=>CH3+CO			4.83E-04	4.0	-2000.0
232. OH+C2H3<=>H2O+C2H2			5.00E+12	.0	.0
233. OH+C2H4<=>C2H3+H2O			3.60E+06	2.0	2500.0
234. OH+C2H6<=>C2H5+H2O			3.54E+06	2.1	870.0
235. OH+CH2CO<=>HCCO+H2O			7.50E+12	.0	2000.0
236. 2HO2<=>O2+H2O2			1.30E+11	.0	-1630.0
Declared duplicate reaction...					
237. 2HO2<=>O2+H2O2			4.20E+14	.0	12000.0
Declared duplicate reaction...					
238. HO2+CH2<=>OH+CH2O			2.00E+13	.0	.0
239. HO2+CH3<=>O2+CH4			1.00E+12	.0	.0
240. HO2+CH3<=>OH+CH3O			2.00E+13	.0	.0
241. HO2+CO<=>OH+CO2			1.50E+14	.0	23600.0

242. HO2+CH2O<=>HCO+H2O2 1.00E+12 .0 8000.0
243. C+O2<=>O+CO 5.80E+13 .0 576.0
244. C+CH2<=>H+C2H 5.00E+13 .0 .0
245. C+CH3<=>H+C2H2 5.00E+13 .0 .0
246. CH+O2<=>O+HCO 3.30E+13 .0 .0
247. CH+H2<=>H+CH2 1.11E+08 1.8 1670.0
248. CH+H2O<=>H+CH2O 5.71E+12 .0 -755.0
249. CH+CH2<=>H+C2H2 4.00E+13 .0 .0
250. CH+CH3<=>H+C2H3 3.00E+13 .0 .0
251. CH+CH4<=>H+C2H4 6.00E+13 .0 .0
252. CH+CO(+M)<=>HCCO(+M) 5.00E+13 .0 .0
Low pressure limit: 0.26900E+29 -0.37400E+01 0.19360E+04
TROE centering: 0.57570E+00 0.23700E+03 0.16520E+04 0.50690E+04
H2 Enhanced by 2.000E+00
H2O Enhanced by 6.000E+00
CH4 Enhanced by 2.000E+00
CO Enhanced by 1.500E+00
CO2 Enhanced by 2.000E+00
C2H6 Enhanced by 3.000E+00
Ar Enhanced by 7.000E-01
253. CH+CO2<=>HCO+CO 3.40E+12 .0 690.0
254. CH+CH2O<=>H+CH2CO 9.46E+13 .0 -515.0
255. CH+HCCO<=>CO+C2H2 5.00E+13 .0 .0
256. CH2+O2<=>OH+HCO 1.32E+13 .0 1500.0
257. CH2+H2<=>H+CH3 5.00E+05 2.0 7230.0
258. 2CH2<=>H2+C2H2 3.20E+13 .0 .0
259. CH2+CH3<=>H+C2H4 4.00E+13 .0 .0
260. CH2+CH4<=>2CH3 2.46E+06 2.0 8270.0
261. CH2+CO(+M)<=>CH2CO(+M) 8.10E+11 .5 4510.0
Low pressure limit: 0.26900E+34 -0.51100E+01 0.70950E+04
TROE centering: 0.59070E+00 0.27500E+03 0.12260E+04 0.51850E+04
H2 Enhanced by 2.000E+00
H2O Enhanced by 6.000E+00
CH4 Enhanced by 2.000E+00
CO Enhanced by 1.500E+00
CO2 Enhanced by 2.000E+00
C2H6 Enhanced by 3.000E+00
Ar Enhanced by 7.000E-01
262. CH2+HCCO<=>C2H3+CO 3.00E+13 .0 .0
263. CH2(S)+N2<=>CH2+N2 1.50E+13 .0 600.0
264. CH2(S)+Ar<=>CH2+Ar 9.00E+12 .0 600.0
265. CH2(S)+O2<=>H+OH+CO 2.80E+13 .0 .0
266. CH2(S)+O2<=>CO+H2O 1.20E+13 .0 .0
267. CH2(S)+H2<=>CH3+H 7.00E+13 .0 .0
268. CH2(S)+H2O(+M)<=>CH3OH(+M) 2.00E+13 .0 .0
Low pressure limit: 0.27000E+39 -0.63000E+01 0.31000E+04
TROE centering: 0.15070E+00 0.13400E+03 0.23830E+04 0.72650E+04
H2 Enhanced by 2.000E+00
H2O Enhanced by 6.000E+00
CH4 Enhanced by 2.000E+00
CO Enhanced by 1.500E+00

```
    CO2             Enhanced by   2.000E+00
    C2H6            Enhanced by   3.000E+00
269. CH2(S)+H2O<=>CH2+H2O                          3.00E+13   .0      .0
270. CH2(S)+CH3<=>H+C2H4                           1.20E+13   .0   -570.0
271. CH2(S)+CH4<=>2CH3                             1.60E+13   .0   -570.0
272. CH2(S)+CO<=>CH2+CO                            9.00E+12   .0      .0
273. CH2(S)+CO2<=>CH2+CO2                          7.00E+12   .0      .0
274. CH2(S)+CO2<=>CO+CH2O                          1.40E+13   .0      .0
275. CH2(S)+C2H6<=>CH3+C2H5                        4.00E+13   .0   -550.0
276. CH3+O2<=>O+CH3O                               2.67E+13   .0  28800.0
277. CH3+O2<=>OH+CH2O                              3.60E+10   .0   8940.0
278. CH3+H2O2<=>HO2+CH4                            2.45E+04  2.5   5180.0
279. 2CH3(+M)<=>C2H6(+M)                           2.12E+16 -1.0    620.0
   Low pressure limit: 0.17700E+51 -0.96700E+01 0.62200E+04
   TROE centering:    0.53250E+00 0.15100E+03 0.10380E+04 0.49700E+04
    H2              Enhanced by   2.000E+00
    H2O             Enhanced by   6.000E+00
    CH4             Enhanced by   2.000E+00
    CO              Enhanced by   1.500E+00
    CO2             Enhanced by   2.000E+00
    C2H6            Enhanced by   3.000E+00
    Ar              Enhanced by   7.000E-01
280. 2CH3<=>H+C2H5                                 4.99E+12   .1  10600.0
281. CH3+HCO<=>CH4+CO                              2.65E+13   .0      .0
282. CH3+CH2O<=>HCO+CH4                            3.32E+03  2.8   5860.0
283. CH3+CH3OH<=>CH2OH+CH4                         3.00E+07  1.5   9940.0
284. CH3+CH3OH<=>CH3O+CH4                          1.00E+07  1.5   9940.0
285. CH3+C2H4<=>C2H3+CH4                           2.27E+05  2.0   9200.0
286. CH3+C2H6<=>C2H5+CH4                           6.14E+06  1.7  10450.0
287. HCO+H2O<=>H+CO+H2O                            2.24E+18 -1.0  17000.0
288. HCO+M<=>H+CO+M                                1.87E+17 -1.0  17000.0
    H2              Enhanced by   2.000E+00
    H2O             Enhanced by   0.000E-01
    CH4             Enhanced by   2.000E+00
    CO              Enhanced by   1.500E+00
    CO2             Enhanced by   2.000E+00
    C2H6            Enhanced by   3.000E+00
289. HCO+O2<=>HO2+CO                               7.60E+12   .0    400.0
290. CH2OH+O2<=>HO2+CH2O                           1.80E+13   .0    900.0
291. CH3O+O2<=>HO2+CH2O                            4.28E-13  7.6  -3530.0
292. C2H+O2<=>HCO+CO                               5.00E+13   .0   1500.0
293. C2H+H2<=>H+C2H2                               4.07E+05  2.4    200.0
294. C2H3+O2<=>HCO+CH2O                            3.98E+12   .0   -240.0
295. C2H4(+M)<=>H2+C2H2(+M)                        8.00E+12   .4  88770.0
   Low pressure limit: 0.70000E+51 -0.93100E+01 0.99860E+05
   TROE centering:    0.73450E+00 0.18000E+03 0.10350E+04 0.54170E+04
    H2              Enhanced by   2.000E+00
    H2O             Enhanced by   6.000E+00
    CH4             Enhanced by   2.000E+00
    CO              Enhanced by   1.500E+00
    CO2             Enhanced by   2.000E+00
```

Ar Enhanced by 7.000E-01			
296. C2H5+O2<=>HO2+C2H4	8.40E+11	.0	3875.0
297. HCCO+O2<=>OH+2CO	1.60E+12	.0	854.0
298. 2HCCO<=>2CO+C2H2	1.00E+13	.0	.0
299. (CH3)2N=>H2+HCN+CH3	4.00E+13	.0	53000.0
300. HCN+OH<=>H2O+CN	3.00E+10	.0	3700.0
301. OH+CN<=>H+NCO	6.00E+13	.0	.0
302. NCO+O2<=>NO+CO2	7.90E+11	.0	.0

NOTE: A units mole-cm-sec-K, E units cal/mole

TECHNOLOGY OPERATIONS

The Aerospace Corporation functions as an "architect-engineer" for national security programs, specializing in advanced military space systems. The Corporation's Technology Operations supports the effective and timely development and operation of national security systems through scientific research and the application of advanced technology. Vital to the success of the Corporation is the technical staff's wide-ranging expertise and its ability to stay abreast of new technological developments and program support issues associated with rapidly evolving space systems. Contributing capabilities are provided by these individual Technology Centers:

Electronics Technology Center: Microelectronics, VLSI reliability, failure analysis, solid-state device physics, compound semiconductors, radiation effects, infrared and CCD detector devices, Micro-Electro-Mechanical Systems (MEMS), and data storage and display technologies; lasers and electro-optics, solid state laser design, micro-optics, optical communications, and fiber optic sensors; atomic frequency standards, applied laser spectroscopy, laser chemistry, atmospheric propagation and beam control, LIDAR/LADAR remote sensing; solar cell and array testing and evaluation, battery electrochemistry, battery testing and evaluation.

Mechanics and Materials Technology Center: Evaluation and characterization of new materials: metals, alloys, ceramics, polymers and composites; development and analysis of advanced materials processing and deposition techniques; nondestructive evaluation, component failure analysis and reliability; fracture mechanics and stress corrosion; analysis and evaluation of materials at cryogenic and elevated temperatures; launch vehicle fluid mechanics, heat transfer and flight dynamics; aerothermodynamics; chemical and electric propulsion; environmental chemistry; combustion processes; spacecraft structural mechanics, space environment effects on materials, hardening and vulnerability assessment; contamination, thermal and structural control; lubrication and surface phenomena; microengineering technology and microinstrument development.

Space and Environment Technology Center: Magnetospheric, auroral and cosmic ray physics, wave-particle interactions, magnetospheric plasma waves; atmospheric and ionospheric physics, density and composition of the upper atmosphere, remote sensing using atmospheric radiation; solar physics, infrared astronomy, infrared signature analysis; effects of solar activity, magnetic storms and nuclear explosions on the earth's atmosphere, ionosphere and magnetosphere; effects of electromagnetic and particulate radiations on space systems; space instrumentation; propellant chemistry, chemical dynamics, environmental chemistry, trace detection; atmospheric chemical reactions, atmospheric optics, light scattering, state-specific chemical reactions and radiative signatures of missile plumes, and sensor out-of-field-of-view rejection.